Molten Salt Corrosion of SiC and Si$_3$N$_4$

Nathan S. Jacobson, James L. Smialek, and Dennis S. Fox
Lewis Research Center
Cleveland, Ohio

November 1988

NASA

MOLTEN SALT CORROSION OF SiC AND Si$_3$N$_4$

Nathan S. Jacobson, James L. Smialek, and Dennis S. Fox
National Aeronautics and Space Administration
Lewis Research Center
Cleveland, Ohio 44135

Abstract

Industrial systems such as heat engines and heat exchangers involve harsh environments. The structural materials are subjected to high temperatures and as well as corrosive gases and condensed phases. Past experience with metal alloys has shown that these condensed phases can be particularly corrosive and are often the limiting factor in the operation of these systems. In a heat engine the most common condensed corrodent is Na$_2$SO$_4$ whereas in a heat exchanger an oxide slag may be present. The primary emphasis of this chapter is on Na$_2$SO$_4$ induced corrosion, however similarities and differences to oxide slag corrosion are also discussed.

The extensive research on corrosion of metal alloys has led to understanding and controlling corrosion for these materials. Currently silicon based ceramics are prime candidates for the applications discussed above. Therefore it important to understand the effects of condensed phase deposits on this emerging class of high temperature materials. Both the thermodynamics and kinetics of the

1

corrosion reactions are discussed. The effect of these
corrosion reactions on the microstructure and strength of the
ceramic is also examined. Finally some control strategies
for corrosion of silicon based ceramics are explored.

I. Introduction

Silicon based ceramics such as SiC and Si_3N_4, and composites based on these materials, are currently prime candidates for high temperature applications such as heat engines and heat exchanger tubes. These ceramics offer a number of advantages which include high strength at temperatures up to 1400°C, good thermal shock resistance, excellent oxidation resistance, light weight, and compositions based on abundant raw materials.

In selecting a material, a prime consideration is its resistance to the chemical environment encountered in the specific application. As mentioned, silicon based ceramics show excellent oxidation resistance. However, actual heat engine or heat exchanger environments often contain more than pure oxygen. Additional species include other oxidants such as chlorine and sulfur dioxide as well as condensed phase deposits. The primary focus of this chapter is on condensed phase deposits. Table I lists potential applications for silicon based ceramics, the temperature ranges, and the possible condensed phase corrodents. Typically these deposits are alkali metal salts and/or oxide slags. It should be noted that corrosion is typically a problem above

the melting point of the deposit. When the deposit is fluid, it spreads readily and rapid transport through the film permits accelerated chemical processes to occur.

It is appropriate to briefly discuss the origin of these deposits. In a heat engine small amounts of sodium ingested from a marine environment or from fuel impurities react with sulfur in the fuel to form sodium sulfate[1]:

$$2NaCl(g) + SO_2(g) + 1/2O_2(g) + H_2O(g) =$$

$$Na_2SO_4(l) + 2HCl(g) \qquad (1)$$
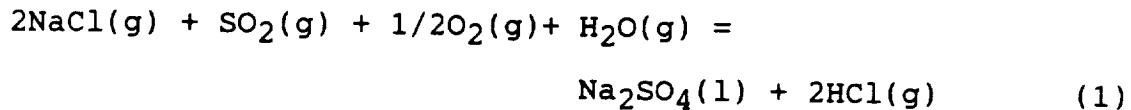
This process and the resulting corrosion can be a problem for metals and has been extensively studied.[2] In addition some fuels may contain vanadium impurities, which form vanadate deposits. Under some conditions these vanadate deposits can be controlled with additives. In a coal combustion situation, a slag containing various oxides forms.[3] In an industrial furnace, such as a fluxing aluminum reclamation furnace, salts may be used as part of the process.[4] Other potential applications include magnetohydrodynamic (MHD) processes, where the gas stream is intentionally seeded with potassium salts[5], and fuel cells which contain molten salts.[6]

Before examining actual corrosion processes, the various types of silicon based ceramics should be discussed. Some common types are listed in Table II. Some types of SiC and Si_3N_4, such as the CVD materials, are extremely pure. However most of the commercial materials contain additives to

promote densification. These additives are often an important factor in the high temperature behavior of these materials.

A survey of research[8-84] on the corrosion of silicon based ceramics is given in Table III, which is divided according to application. The earlier studies (1952-1974) center on the use of molten salts as an etchant. These studies show that basic molten salts selectively attack structural discontinuities in SiC. This observation is important in understanding the corrosive action of molten salts in actual applications. Most of the subsequent research in ceramic corrosion deals with heat engines. This is because corrosion of metal alloys in engines had proven to be such a formidable problem.[2] Most of these studies center on Na_2SO_4 induced corrosion of SiC and Si_3N_4; only limited information on vanadate induced corrosion of SiC and Si_3N_4 was found.

Table III includes headings for the type of ceramic examined, the corrodent, and the experimental technique. Three major experimental methods are listed in the "Technique" column--burner tests wherein the flame is seeded with salt, laboratory crucible tests, and laboratory film tests. The techique used depends on the application being modeled and the type of information sought. Burner tests may accurately model the actual application, but it is difficult

to control the experimental parameters and determine a chemical mechanism of corrosion. Furthermore, these tests require much more apparatus than a laboratory study. In a laboratory crucible test, the sample is covered by a deep melt. These types of studies dominated the early corrosion literature. This type of test may be appropriate for a study of coal slag corrosion, but for a heat engine corrosion study, the oxygen potential at the melt/specimen interface may be unrealistically low. In a laboratory film study the specimen is coated with a film of the corrosive salt. The various parameters, such as gas composition at the melt/specimen interface, can then be more easily controlled. Current studies aimed at a fundamental understanding of heat engine corrosion center on thin films.

The primary emphasis of this chapter will be corrosion by sodium sulfate in heat engines. However many of the principals for this type of corrosion apply to other types of corrosion. Where possible, unifying concepts will be discussed.

II. Chemistry

Silicon based ceramics are inherently unstable in oxygen and rely on a thin film of SiO_2 for oxidation protection.

This film provides good protection to about 1500°C.
Corrosion processes may destroy this oxide film, exposing the
material to extensive attack.

Consider corrosion by sodium sulfate in a heat engine
application. This occurs in two steps--deposition of Na_2SO_4
on an engine part and the actual corrosion process. As
mentioned, sodium sulfate forms by Equation (1). Typically
corrosion occurs in a temperature regime bounded by the
melting point of sodium sulfate (884°C) and the dew point for
deposition of sodium sulfate. The dew point is a function of
pressure and concentration and can be calculated from
thermochemical equilibrium codes.[85] Dew points for a variety
of conditions are shown in Table IV. Higher operating
temperatures decrease the likelihood of deposition, since no
deposit will form if the thermodynamic dew point is exceeded.
However higher operating pressures increase the likelihood of
deposition since higher pressures increase the dew point.
Since future heat engines are expected to operate at both
higher temperatures and pressures, the possiblity of
deposition and subsequent attack must be carefully
considered.

Figure 1(a) shows a coupon of SASC (B,C) exposed in a
burner rig with no salt. Essentially no attack has occurred
and the coupon is nearly indistinguishable from the starting
material. However, when only 4 ppm sodium as sodium chloride

is added to the flame, a large glassy deposit forms as shown in Figure 1(b).[47] This glassy material is shown as a polished cross section in Figure 2. The associated x-ray maps show an even distribution of Si, O, and Na, suggesting a sodium silicate glass. Thus the likely reaction scheme is:

$$SiC(s) + 3/2O_2(g) = SiO_2(s) + CO(g) \qquad (2)$$

$$xSiO_2(s) + Na_2SO_4(l) = Na_2O \cdot x(SiO_2)(l) + SO_3(g) \qquad (3)$$
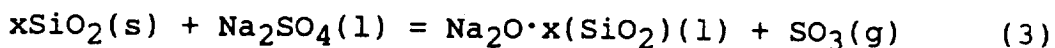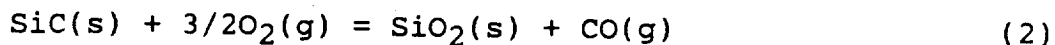
The important point to note is that the solid, protective silica layer has been dissolved to a form a liquid, non-protective sodium silicate layer. The faster transport rates through this liquid layer allow extensive corrosion of the ceramic. The Na_2O-SiO_2 phase diagram[86] is shown in Figure 3. Note that a small amount of Na_2O would be expected to form some liquid silicate.

Reaction (3) can be written more fundamentally as:

$$Na_2SO_4(l) = Na_2O(s) + SO_3(g) \qquad (4)$$

$$xSiO_2(s) + Na_2O(s) = Na_2O \cdot x(SiO_2)(l) \qquad (5)$$
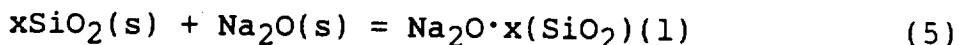
This indicates that the key reactant is Na_2O. The chemical activity of Na_2O [$a(Na_2O)$] is an important parameter. In analogy with Lewis acid-base concepts, a high $a(Na_2O)$ salt is termed a basic molten salt and a low $a(Na_2O)$ is termed an acidic molten salt. From reaction (5) a threshold $a(Na_2O)$ for silica dissolution can be calculated. The stable silicates, as a function of $a(Na_2O)$ at 1000°C, are shown in Figure 4.[87] Note that silica dissolution only

8

occurs for larger $a(Na_2O)$. This type of dissolution, wherein the silica accepts an oxide anion, is termed basic dissolution. Unlike other oxides, silica does not undergo acidic dissolution, wherein the oxide donates an oxide anion to the melt.[88] Thus a well defined regime for silica dissolution as a function of $a(Na_2O)$ and temperature can be easily calculated.

This regime is calculated as follows. The important boundary to examine is between SiO_2 and the first stable silicate -- $Na_2O\cdot2(SiO_2)$, as shown in Figure 2. Taking the activity of SiO_2 and the activity of $Na_2O\cdot2(SiO_2)$ to both be unity, the minimum $a(Na_2O)$ for dissolution can be calculated from reaction (5) with $x = 2$:

$$RT \log a(Na_2O) = G(reaction\ (5)) \qquad (6)$$

Here R is the gas constant and T is temperature in degrees Kelvin. As reaction (4) shows, the activity of Na_2O is set by the partial pressure of $SO_3(g)$ -- $p(SO_3)$. Taking the activity of Na_2SO_4 to be unity:

$$G = - RT \ln p(SO_3)\ a(Na_2O) \qquad (7)$$

Thus from the minimum $a(Na_2O)$ for dissolution, a maximum $p(SO_3)$ can be calculated. This is shown as an upper boundary for corrosion in Figure 5(a) and (b).[53] Using the NASA Chemical Equilibrium Code[85], the partial pressure of SO_3 in a heat engine can be calculated. The parameters which determine this include temperature, pressure, and sulfur

content in the fuel. The results for Jet A fuel (~0.05% S) are shown in Figure 5(a) and the results for No. 2 Diesel fuel (~0.5% S) are shown in Figure 5(b). When the $p(SO_3)$ in the engine is below the upper boundary of $p(SO_3)$ for dissolution, corrosion is predicted. Note that with Jet A fuel this occurs at about ~995°C, whereas with No. 2 Diesel fuel this occurs at about ~1080°C.

As mentioned, corrosion occurs between well defined temperature limits. The lower limit is the melting point for Na_2SO_4--884°C. The upper limit is the dew point for Na_2SO_4 deposition, as shown in Table IV. These are shown on Figures 5(a) and (b). Note that dissolution can occur for the higher sulfur fuel above the dew point. Thus corrosion is not predicted for No. 2 Diesel fuel under the conditions described by Figures 5(a) and 5(b).

This type of diagram can be generated for a variety of pressures and sodium and sulfur concentrations.[53] The figures shown here are for 4 atm total pressure, which corresponds to the NASA burner rig used for these studies. To test these calculations, quartz specimens were run in a burner rig under conditions corresponding to points (A) and (B) in Figures 5(a) and (b). Visual examination of the specimens suggested the higher sulfur fuel caused only limited corrosion, as shown in Figure 6. These coupons were also tested for water soluble silicon, which indicates the

10

presence of sodium silicate. The coupons corroded in Jet A fuel for only 1 hr with 2 ppm Na had 0.16 ± 0.10 mg Si/cm^2, whereas the coupons corroded for 5 hrs in No. 2 Diesel fuel with 2 ppm Na had 0.003 ± 0.003 mg Si/cm^2. These data are consistent with the predictions.

It has been shown that corrosion occurs by dissolution of the SiO_2. The conditions for dissolution are determined by the activity of Na_2O, which can be calculated for the particular condition. These general principles can be extended to other salt systems. In the case of Na_2CO_3, $p(CO_2)$ sets the activity of Na_2O:

$$Na_2CO_3(l) = Na_2O(s) + CO_2(g) \tag{8}$$
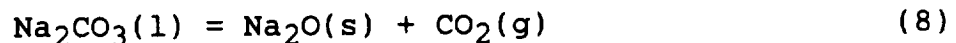
Na_2CO_3 tends to dissociate more than Na_2SO_4 and hence is a more basic molten salt. Indeed, it has been shown that the Na_2CO_3 tends to attack silica much more readily than Na_2SO_4.[45] In the case of NaCl and water vapor, Na_2O can form by the following reaction[89]:

$$2NaCl(v) + H_2O(v) = Na_2O(s) + 2HCl(g) \tag{9}$$
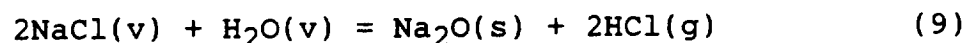
In this case $a(Na_2O)$ would be set by the vapor pressures of the other three species.

It should be noted that other compounds in the environment and/or the material under consideration may influence the activity of Na_2O. This is well documented for

metallic alloys.[2] In the case of silicon carbide, a common additive is carbon. It has been shown that carbon can drive a melt basic[53] by the following reactions:

$$Na_2SO_4(l) + 2C = Na_2S + 2CO_2 \tag{10}$$

$$Na_2S + 3Na_2SO_4 = 4Na_2O + 4SO_2 \tag{11}$$
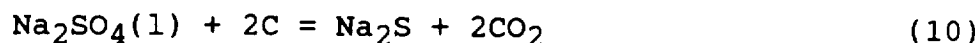
This fact explains the more extensive corrosion of SiC containing carbon additives compared to SiC with other additives. Additional deposits can also alter the activity of Na_2O. As mentioned, vanadium oxides are a common fuel impurity and can deposit as sodium vanadate along with sodium sulfate. This may decrease $a(Na_2O)$ thus creat a more acidic deposit.[2]

Another important variable is the potential of gaseous oxygen at the melt/ceramic interface. In a deep melt, this potential can be quite low. It is well known that SiC and Si_3N_4 undergo a transistion from passive oxidation (to SiO_2) to active oxidation (to SiO) at sufficiently low oxygen potentials.[21] Therefore some investigators[21,75] have proposed that the corrosion mechanism in melts with low oxygen potentials involves active oxidation:

$$SiC(s) + O_2(g) = SiO(g) + CO(g) \tag{12}$$
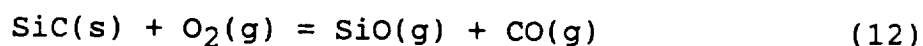
This mechanism can explain excessive bubbling and consumption of the material in a deep melt.

Another mechanism is based on the Na present in these salts. It is well known that Na can induce devitrification

12

in amorphous SiO_2.[46] The resultant volume change can cause cracking and a breakdown of the protective SiO_2 layer. Thus even acidic salts may lead to degradation of SiO_2 protected ceramics via this mechanism.[39-41,52]

The discussion so far has centered on fairly simple sodium containing salt deposits. In the case of a coal slag, the situation becomes much more complex. Slags are composed of roughly eight different oxides and a(Na_2O) can therefore no longer be used as a simple index of basicity. A relative measure of basicity is given by the ratio of basic oxides to acidic oxides. Table V gives a typical basic and acidic coal slag composition.[62] The possible corrosion mechanisms by a basic coal slag have recently been discussed.[63] The three mechanisms disscussed are passivation via SiO_2 formation, dissolution of SiO_2 by the basic slag, and formation of localized Fe-Ni-silicides. The first two mechanisms are similar to those discussed for corrosion by Na_2SO_4. The last mechanism occurs in a deep melt (≥ 100 μm) where the oxygen potential is low enough that the silicon material does not oxidize and reactions such as the following occur:

$$13SiC + 5Fe(slag\ matrix) = Fe_5Si_{13} + 13C \qquad (13)$$
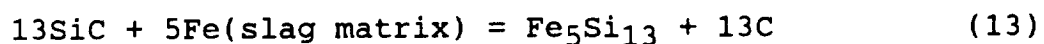
Thus the presence of transition metal oxides in slags can lead to some important corrosion mechanism differences between slag induced corrosion and Na_2SO_4 induced corrosion.

III. Reaction Kinetics

An understanding of a corrosion mechanism includes more than just the major chemical reactions. It also includes a knowledge of the reaction rates and rate controlling steps. For heat engine applications, these are best studied through carefully controlled laboratory experiments using thin salt films. The thin salt films are airbrushed from a saturated aqueous solution onto a ceramic coupon, and the coated coupon is placed in a furnace with a well defined gas environment. The reaction can be followed with several techniques. The most common is thermogravimetric analysis, where the weight change is continuously monitored as a function of time. Another technique is chemical analysis of the corrosion scales at various time intervals. The corrosion products from silicon based ceramics are particularly well suited for chemical analysis because they consist of sodium silicate and sodium sulfate, which are both water soluble, and silica, which is only HF soluble. When a clear distinction occurs between these two phases, the authors have found the technique outlined in Figure 7 to provide useful information.[45]

In addition to following the chemical reaction with thermogravimetric and chemical analysis techniques, the

14

morphology of the reaction products can be examined after various reaction times. Product layers can be selectively removed by water or HF leaches and the resultant exposed surfaces examined. Polished cross sections show the distribution of elements throughout the product layers. Non-aqueous lubricants and solvents must be used to preserve the water soluble phases.

Consider first the chemical kinetics of the corrosion by sodium carbonate.[46,51] As mentioned, this is a basic molten salt which readily dissolves the protective oxide layer. Figures 8(a) and 8(b) are thermogravimetric and chemical analysis kinetic curves, respectively, for the reaction of SASC (B,C) with Na_2CO_3 at $1000^\circ C$. There are three distinct reaction stages. Stage I is characterized by a rapid weight loss for the first few minutes of reaction and is attributed to the coupled oxidation of SiC and dissolution of the resultant oxide:

$$SiC(s) + 3/2O_2(g) = SiO_2(s) + CO(g) \qquad (14)$$

$$xSiO_2(s) + Na_2CO_3(l) = Na_2O \cdot x(SiO_2)(l) + CO_2(g) \qquad (15)$$
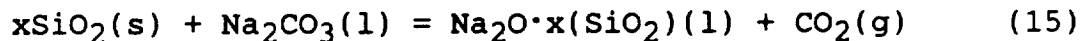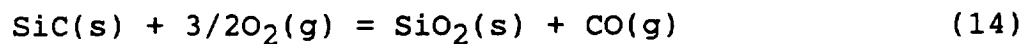
If x is taken as 1 and the amount of Na_2CO_3 taken to be the typical loading of 2.5 mg/cm^2, a weight loss can be estimated. This was quite close to that measured. A number of different types of Si, SiC, and Si_3N_4 ceramics have been

examined. Each exhibited a Stage I weight loss close to that calculated from reactions (14) and (15), and analogous reactions for Si and Si_3N_4.[51]

Next consider reaction Stage II. This is a period of slow weight gain. In Figure 8(a) this appears somewhat parabolic, suggesting mass transport is rate limiting. Examination of Figure 8(b) suggests that Stage II is characterized by the formation of SiO_2. However, this rate of growth is substantially faster than simple oxidation. Microstructural observations indicate that this SiO_2 does not form as a dense, protective layer, but rather in non-protective patches. This accounts for the rapid growth rates. It may also be that small amounts of Na dope the SiO_2, leading to more rapid transport rates.[28,29,39-41] As time progresses, this lower layer becomes dense and seals off the SiC from further reaction in Stage III. Figure 9 is a polished cross section which shows this layered structure.

Mayer and Riley[28] have focused their attention on the time required to reach Stage III for various temperatures and amounts of Na_2CO_3. They have found a correlation between the point at which the reaction terminates and a Na_2O-to-SiO_2 ratio close to the liquidus (Figure 3).

Figure 10 shows a thermogravimetric curve for the reaction of SSN (Y_2O_3) and Na_2CO_3. As discussed, Stage I is

16

essentially the same for all types of SiC and Si_3N_4.
However, note that Stage II for SSN (Y_2O_3) is substantially
slower than Stage II for SASC (B,C). A variety of SiC and
Si_3N_4 ceramics were examined and it was found that both the
rate and extent of Stage II is dependent on the particular
ceramic and/or additive. The generally slower rates for
Si_3N_4 are attributed to either hindered nitrogen escape
through the product layers and/or the possibility of the
formation of a more protective Si_2O_2N layer.[51] The
differences between the various types of Si_3N_4 are attributed
to the migration of the additives into the corrosion layer
which alters its transport properties.

The Na_2CO_3 corrosion kinetics provide a good basis for
examining Na_2SO_4 corrosion. As mentioned, this is a more
acidic molten salt and will not readily dissolve SiO_2.
Figure 11 shows thermogravimetric data for HIP RBSN +
Na_2SO_4/O_2. Without an overpressure of $p(SO_3)$, the $a(Na_2O)$
would be expected to vary. Electrochemical measurements show
that in a Na_2SO_4/O_2 system[53], $a(Na_2O)$ varies from 5.6×10^{-14}
to 1×10^{-12}. Referring to Figure 4, this is a region where
SiO_2 would not be attacked. This explains the slow rates of
reaction observed in Figure 11. The slow weight loss is
essentially all due to the vaporization of Na_2SO_4, which has
the same rate of weight loss when applied to an inert
platinum coupon. There is also a limited amount of

dissolution, as some local regions of the melt are basic. This 30-40 hr period of weight loss was the same for all types of Si_3N_4 examined.

Figure 12 shows thermogravimetric data for the reaction of SASC (B,C) and Na_2SO_4/O_2. This is substantially different than the reaction of Si_3N_4 + Na_2SO_4/O_2. Indeed it has a similar appearance to the SASC (B,C) or SSN (Y_2O_3) + Na_2CO_3 reaction. This type of SiC contains about 3% excess carbon.[90] It was pointed out in the previous section that carbon tends to drive Na_2SO_4 more basic. This accounts for the fact that Figure 13 shows kinetics similar to those observed for corrosion by Na_2CO_3.

Finally consider corrosion reactions by a strongly acidic salt--$Na_2SO_4/0.1\%$ SO_3-O_2. In this case the activity of Na_2O should be constant at 5×10^{-16}, a value clearly in region of stability for SiO_2. Table VI shows the chemical analysis results for 48 hrs at $1000^\circ C$. Note that no silicate was observed for all materials except SASC (B,C). The reasons for this are due to the effect of carbon on melt basicity. The carbon in the SiC creates locally basic conditions at the melt bottom, and the SO_3 above the Na_2SO_4 deposit creates acidic conditions at the top of the melt. Thus dissolution occurs at the bottom of the melt and precipitation of SiO_2 and regeneration of the Na_2SO_4 occurs at the top of the melt, as described in Figure 13. These

18

self-sustaining reactions are termed "fluxing" and well known from the hot corrosion of metals.[2] Due to the fluxing mechanism, the microstructure shown in Figure 14 forms, which shows sodium silicate and sodium sulfate in a large portion of the product layer. This is indicated by the sodium and sulfur elemental maps, respectively.

The preceeding discussion of kinetics in molten salt corrosion has dealt with carefully controlled experiments with a thin film of salt. It is appropriate to comment on how these relate to actual cases of molten salt corrosion. The laboratory studies have shown that coupled oxidation-dissolution processes, such as reactions (12) and (13), are quite rapid. Thus the thick glassy layer observed in Figure 1 could form quite rapidly. Under conditions where a basic molten salt is continuously deposited, extensive corrosion could occur. Under conditions where such a salt is only deposited for a limited amount of time, a healing layer of SiO_2 may eventually develop. It is also important to note that carbon--either as an additive in the ceramic or deposited in the combustion situation--can drive a normally non-reactive acidic salt to a reactive basic salt.

Kinetic studies of reactions in deep melts are generally performed by withdrawing the specimens at various time intervals, removing the salt and products, and weighing the specimen.[22,80-84] In general, partial removal of the

products is obtained by treatment with water and total

removal is obtained by treatment with an HF solution.

Tessler et. al.[22] have observed ~30% weight loss of SiC in

several hours and ~30% weight loss of Si_3N_4 in 40-60 hrs. in

a Na_2SO_4 melt. Note the more rapid dissolution of SiC

follows the same trend as observed with the thin film

studies. Shimada et. al.[80-83] have examined the kinetics of

corrosion of SiC and Si_3N_4 in various sulfates and carbonates

of lithium, sodium, and potassium. Under some conditions,

they have found SiC to corrode more slowly than Si_3N_4. This

suggests that corrosion in deep melts is a complex function

of the salt and ceramic and very likely parameters such as

melt depth.

IV. Microstructural Changes

The discussion thus far has centered on the chemical

reactions involved in the corrosion of SiC and Si_3N_4. The

net effect of these reactions is consumption of the ceramic

and it is important to understand the manner in which this

occurs. Possible modes of attack are uniform surface

recession or attack in localized regions. If the attack

occurs in localized regions, it is important to determine the

unique features of these regions. A knowledge of the attack
mode should aid in understanding how corrosion effects the
performance of the ceramic in service.

The corroded microstructure of the ceramic must be
examined without the interference of the corrosion products.
This can be done with two methods. One is by examination of
a polished cross section, as shown in Figures 9 and 14.
Another is by cleanly removing the corrosion scale. In the
case of SiC this can be done with HF, which dissolves the
entire corrosion scale but does not attack the SiC. Figure
15 shows a sequence of the as-received SiC, the corroded SiC
with the product layer, and the corroded SiC with the product
layer cleanly removed.

As Figure 15 shows, molten salt corrosion of SiC leads
to severe grain boundary attack and pitting.[49,50] This type
of attack has been observed in oxidation[50,91] and corrosion
by deep melts.[24] Pitting is particularly important since the
strength of a ceramic is often quite dependent on surface
finish. Table VII lists the pit density corresponding to
three different salt systems. In each case the specimen was
corroded for 48 h at 1000°C with 2.5 mg salt/cm^2 applied as a
film. These results correlate to the extent of reaction
discussed in the chemistry section. The Na_2CO_3 case shows
the least amount of pitting, since a healing SiO_2 layer forms
rapidly in this reaction. The Na_2SO_4/SO_3 case is the fluxing

situation and leads to the most extensive corrosion. This is reflected in the high pit density data.

The corrosion reactions (2) and (3) involve the release of gases. These escape through the scale as bubbles. These bubbles are 1-10 μm in diameter and are observed on all samples. Furthermore, they are often correlated with pits. Figure 16 shows a series of micrographs taken of the sodium silicate layer, the silica layer, and the SASC (B,C) substrate on a sample corroded with Na_2CO_3. Note the larger pits correlate directly with a bubble. It appears that when a gas bubble forms it exposes a fresh portion of SiC, which is susceptible for further attack. This is shown schematically in Figure 17 for Na_2CO_3 corrosion. Evidence suggests that a a similar mechanism is operative for Na_2SO_4.[50]

The question remains as to why bubbles form at some points in the melt leading to pits, whereas other areas exhibit limited bubble formation and pitting. The is quite apparent with pitting by Na_2CO_3. One possible explanation is a localized cell situation, analogous to aqueous pitting corrosion of metals. There are a number of parallels between the two cases. Both the aqueous media and the molten salt are conductors. Metals and SiC are also conductors. Furthermore the pitting morphology is similar in both cases. Pitting of metals occurs due to local regions of oxygen

22

depletion (anodes) and excess oxygen (cathodes). It is quite likely that inhomogenieties in the salt film can create a similar situation in the SiC case.

The attack morphology of Si_3N_4 shows some interesting differences as compared to that of SiC. The corrosion scale on Si_3N_4 may also be removed with HF, however HF can attack the grain boundary phase. Therefore a mild HF treatment (15 min, 10% HF, 60°C) must be used to obtain an accurate picture of the attack morphology. A sequence based on this treatment for Si_3N_4 is shown in Figure 18.[55] Note that the grain boundaries show substantial attack and pitting is of limited importance. This is consistent with the proposed electrochemical model for SiC, since Si_3N_4 is more insulating than SiC. It is well known that the refractory oxide additives in Si_3N_4 form a glassy grain boundary phase. This grain boundary phase is readily altered by the molten salt corrosion process. Figure 19 shows a polished cross section of Si_3N_4. The important point is the yttrium map, which shows the outer 5-10 μm of Si_3N_4 is depleted in yttrium, which has migrated into the corrosion scale. This migration of yttrium has been observed in simple oxidation[92] and in corrosion by several investigators.[39-41,51,52] In addition to this the corrodents -- Na and S -- penetrate into the ceramic, very likely along grain boundaries. This was shown with some earlier electron microprobe measurements[22] and has

been shown recently with Secondary Ion Mass
Spectrometry (SIMS).[55] These SIMS results are shown in Figure
20. Note the Y depletion zone and the high levels of Na well
into the sample. Even sulfur shows some limited penetration.

In summary, molten salt corrosion causes some dramatic
microstructural effects on the microstructure of SiC and
Si_3N_4. In the case of SiC this effect is primarily pitting.
In the case of Si_3N_4 this is primarily grain boundary attack.

Coal slag corrosion produces complex microstructural
changes, which are quite sensitive to slag chemistry and the
specific ceramic. As mentioned, in some cases metal
silicides form, which lead to surface pits.[62,64,66] In other
cases slag penetration into the ceramic is the dominant mode
of attack, particularly with Si_3N_4.[62] In still other cases,
fairly even surface recession was observed.[62] The next step
is to assess how these microstructural changes affect the
operation of these components in service.

V. Strength Degradation

As mentioned, the surface finish of a ceramic often has
a major effect on its strength. Surface flaws may act as
failure origins, leading to lower strengths compared to the

same material with a uniform surface finish. The severe

pitting observed in SiC would thus be expected to have an

effect on the strength of this material.

Figure 21 shows the strength of SASC (B,C) for several

different corrosion treatments.[49] Note that each corrosion

treatment decreases the strength below the as-received value.

Since the strengths of ceramics tend to show a substantial

standard deviation, a Student's t-test was performed to

determine if the observed strength reductions were

significant. In all but the Na_2CO_3 case significant strength

reductions were observed.

The relative strength reductions are consistent with the

extent of chemical reaction for each of the laboratory tests.

Although Na_2CO_3 reacts most readily with SiC, the reaction

was shown to be rapid, and a protective SiO_2 layer forms

before any extensive reaction and pitting can occur. The

Na_2SO_4 reactions are somewhat more severe. It has been shown

that Na_2SO_4/SO_3 establishes a self-sustaining series of

reactions and leads to extensive corrosion. This leads to

severe pitting and the greatest strength reduction. The

Na_2SO_4/O_2 system appears to lie between the Na_2CO_3 case and

the Na_2SO_4/SO_3 case.

Other types of SiC were also tested in the burner rig.

The resultant strength degradations are shown in Figure 22.[55]

These types of SiC are described in detail in Table II. The greatest strength degradation is for RBSC which may be due to the free Si phase in this material, which is readily attacked by the molten salt. The common behavior of all types of SiC confirms that corrosion of SiC is due to the dissolution of the SiO_2 layer by basic molten salts and the tendency of SiC to pit.

In order to further understand this strength degradation the fracture origins of numerous specimens were examined. In nearly all cases these were corrosion pits at the surface. Figures 23 and 24 show some representative fracture origins for SASC (B,C) tested in the furnace and burner rig, respectively. Note the deep pitting and grain boundary attack.

From fracture mechanics the fracture stress (σ_f) is controlled by an idealized flaw as follows:

$$\sigma_f = Z/Y \; K_{IC}/(a)^{1/2} \qquad (16)$$

Here Z is the flaw shape parameter, Y is a geometric factor, and K_{IC} is the fracture toughness. The measurement (a) is the depth of an atomically sharp crack. Although corrosion pits are not strictly atomically sharp cracks, a plot of σ_f vs $1/(a)^{1/2}$ (Figure 25) gives a roughly linear dependence with a slope close to that observed from previous fracture toughness measurements.[49] This verifies that corrosion pit depth does indeed control strength.

As discussed in the previous section, corrosion of Si_3N_4 by molten salts leads to a different attack morphology that is dominated by grain boundary attack. It should also be noted that some types of Si_3N_4 show a strength decrease due to softening of the glassy grain boundary phase at elevated temperatures. In examining these types of materials for corrosion induced strength degradation, the effect of strength degradation from a simple heat treatment must be separated from the effect of the molten salt.

Figure 26 shows the room temperature strengths for two types of sintered Si_3N_4.[54] The material with Y_2O_3 and Al_2O_3 shows a strength degradation from a simple 1000°C oxidation and a further strength degradation from a corrosion treatment. The Student's t-test shows that both are significant. The material with Y_2O_3 shows a only a limited strength degradation from a 1000°C heat treatment, which is not statistically significant. However, it does show a significant strength reduction from the corrosion treatment.

Figure 27 shows a typical fracture origin for a corroded Si_3N_4 sample. Although failure occurred near the surface, it was not associated with a deep pit, as in the SiC case. It may be that attack of the grain boundary phase by the molten salt is the likely reason for the failure origin.

The results of high temperature strength testing are complex and point out the difficulties inherent to current

types of Si_3N_4. These are shown in Figures 28(a) and (b). Apparently the actual testing of these materials at elevated temperatures causes a strength decrease of magnitude close to that from the corrosion treatment. In summary, molten salt corrosion decreases the room temperature strengths of Si_3N_4. However, high temperature strengths of these materials are less than the room temperature strengths regardless of their exposure.

This discussion has centered on strength degradation due to thin film and burner corrosion exposures. However deep melts cause similar strength reductions.[23,24,43,44,82,83] Bourne and Tressler have shown an increase in critical flaw size and in most cases a decrease in fracture toughness due to molten exposure of Si_3N_4.[23] Sato et. al.[83] have also observed large increases in flaw sizes in Si_3N_4 due to K_2CO_3 and K_2SO_4 deep melt exposure.

The information presented so far deals with the simple fast fracture strength of SiC and Si_3N_4. To fully understand the effects of molten salt corrosion on these materials, time dependent mechanical properties must be considered as well. Loaded C-ring specimens of SASC (B,C) show shorter time to failure in a NaCl containing environment than a pure oxidizing environment.[76] Recent studies on have shown

enhanced slow crack growth in both SiC and Si_3N_4.[37,57] This is attributed to the formation of a low melting silicate at the crack tip, creating less resistance to crack propogation.

There is a good deal of information on the effects of coal slags on strengths of various ceramics.[59-68] The extent of strength degradation appears to be quite dependent on the type of ceramic and the slag and it is difficult to identify any general trends. As mentioned, in an acidic slag only limited dissolution occurs and either pitting or slag penetration may lead to strength degradation. Basic slags lead to rapid rates of material consumption and may also exhibit pitting. In general wherever pitting was observed, strength degradations were also observed.

VI. Possible Solutions

There are several possible solutions to the hot corrosion problem for silicon base ceramics. Either the salt deposit and/or the protective silica scale can be modified. The salt deposit can be modified by creating more acidic conditions. Figure 5(b) shows that a higher sulfur fuel can create a more acidic salt and limit corrosion. However, in practice this may not be feasible. There are other

considerations which may preclude the use of a higher sulfur fuel. Furthermore, even if the overall conditions are acidic, locally basic regions may occur within the melt.

The second approach is to modify the protective silica layer. Federer[75] has suggested adding Al_2O_3 to produce $Na_2O \cdot SiO_2 \cdot Al_2O_3$ scales that are less susceptible to liquid formation. The next step beyond modification of the SiO_2 scale is the application of an additional protective coating. Recent work at Solar Turbines, Inc.[93] has shown that a plasma sprayed mullite coating provides a promising protective layer for both heat exchanger tubes and heat engine components. Mullite shows a good match of thermal expansion with SiC, and the stochiometric $2(SiO_2) \cdot 3(Al_2O_3)$ compound with no excess SiO_2 shows good corrosion resistance. One difficulty with these coatings is their porosity. However if thicker layers are applied and/or the porosity is closed off, minimal salt penetration occurs. Some results[94] are shown in Figure 29. The coated samples show Na_2SO_4 deposition but no silicate formation or attack (Figure 29(a)) for a 20 hr exposure. The uncoated samples exhibit the typical massive sodium silicate products discussed previously (Figure 1 and 29(b)).

30

VII. Conclusions

The Na_2SO_4 induced corrosion of silicon based ceramics has been discussed. The key reactant is Na_2O which can be derived from a number of salt deposits. This reacts with the SiO_2 scale and forms liquid $Na_2O \cdot x(SiO_2)$, which is not protective, and thus the ceramic is exposed to extensive attack. The dissolution reaction is controlled by a threshold value of Na_2O activity [$a(Na_2O)$]. When this value is greater than a certain level (i.e. basic molten salt), the dissolution reaction readily occurs. In some combustion conditions this $a(Na_2O)$ can be calculated and the possibility of corrosion predicted. It should be noted, however, that $a(Na_2O)$ often shows a complex dependence on gas atmosphere and additives in the ceramic material. Carbon, in particular, tends to drive $a(Na_2O)$ to higher levels. In complex systems such as coal slags, silicon based ceramics show the same rapid dissolution if the system is sufficiently basic.

The kinetics of these corrosion processes are complex, involving several reaction steps. For thin films of Na_2CO_3 and Na_2SO_4, the reaction sequence consists of rapid dissolution and eventual formation of a protective SiO_2 layer when the available Na_2O is consumed. In a combustion situation, where there is a continuous source of Na_2O, this

silica layer may never form and the ceramic may dissolve entirely in the salt.

The precise type of attack is important in assessing how the materials respond to corrosion in service. Molten salts dramatically pit SiC. The source of these pits are attributed to bubble formation during the reaction process and a possible electrochemical reaction scheme. The corrosion process in Si_3N_4 leads to extensive grain boundary attack, an additive depletion layer, and Na and S penetration.

These microstructural changes lead to changes in the mechanical properties of the ceramic. SiC shows strength decreases which are directly attributable to the corrosion pits. In general, Si_3N_4 shows a room temperature strength decrease due to molten salt corrosion. However, at higher temperatures the effect is not as clear due to strength losses intrinsic to many types of Si_3N_4. Time dependent mechanical properties are also degraded by corrosion. In the case of slow crack growth, the solid oxide at the crack tip becomes a liquid due to the interaction with Na and there is less resistance to crack growth.

For coal slags, the microstructural changes are in the form of pits associated with metal silicide formation, slag penetration, and/or surface recession. In general, when pits form, a strength degradation occurs.

32

Solutions to the hot corrosion problem for silicon based ceramics center on creating a less basic salt deposit and/or altering the protective oxide scale. Currently it appears application of a dense refractory oxide protective coating is the most effective.

REFERENCES

1. F.J. Kohl, C.A. Stearns, and G.C. Fryburg, Sodium Sulfate: Vaporization and Role in Corrosive Flames, Metal-Slag-Gas Reactions and Processes, (Z.A. Foroulis and W.W. Smeltzer, eds.) The Electrochemical Society, Pennington, NJ, 1975, p. 649.

2. F.S. Pettit and C.S. Giggins, Hot Corrosion, Superalloys II, (C.T. Sims, N.S. Stoloff, and W.C. Hagel, eds.) Wiley & Sons, New York, 1987, p.327.

3. E. Raask, Mineral Impurities in Coal Combustion, Hemisphere Publishing Company, Washington, 1985.

4. A.D. Russell, C.E. Smeltzer, and M.E. Ward, "Waste Heat Recuperation for Aluminum Furnaces," GRI-81/0187, Solar Turbines Inc., San Diego, CA, 1983.

5. J.E. Bennett, F.J. Kohl, C.A. Stearns, G.C. Fryburg, and J.A. Burkhart, "Preliminary Evaluation of the Role of K_2S in MHD Hot Stream Seed Recovery," NASA TM-79114, DOE/NASA/2674-79/1, 1979.

6. H.S. Hsu, J.H. DeVan, and M. Howell, Corrosion of Iron in Molten Carbonates at 650°C, Fundamental Aspects of High Temperature Corrosion--II, The Electrochemical Society, Pennington, NJ, 1986, p. 86.

7. G.K. Watson, T.J. Moore, and M.L. Millard, "Effect of Hot Isostatic Pressing on Reaction-Bonded Silicon Nitride," J. Am. Ceram. Soc., 67[10]: C-208 (1984).

8. F.H. Horn, "Screw Dislocations, Etch Figures, and Holes," Philos. Mag., 43: 1210 (1952).

9. J.W. Faust, The Etching of Silicon Carbide, Silicon Carbide: A High Temperature Semiconductor, (J.R. O'Connor and J. Smiltens, eds.) Pergamon Press, New York, 1959, p. 403.

10. S. Amelinckx, G. Strumane, and W.W. Webb, "Dislocations in Silicon Carbide," J. Appl. Phys., 31[8]: 1359 (1960).

11. T. Gabor and R. Stickler, "Chemical Etching Studies and Transmission Electron Microscopy of Silicon Carbide," Nature, 199[489]: 1054 (1963).

12. T. Gabor and V.J. Jennings, "The Effect of Stirring on the Etching Characteristics of Silicon Carbide," Electrochem. Technol., 3: 31 (1965).

13. J.W. Faust, Jr. and H.M. Liaw, Tables of Etchants for SiC, Silicon Carbide - 1973, (R.C. Marshall, J.W. Faust Jr., and C.E. Ryan, eds.) University of South Carolina Press, Columbia, SC, 1974, p. 657.

14. S.C. Singhal, Corrosion Behavior of Silicon Nitride and Silicon Carbide in Turbine Atmospheres, Proceedings of the 1972 Tri-Service Conference on Corrosion, MCIC-73-19, Metals and Ceramics Information Center, Battelle Labs, Columbus, OH, 1973, p. 245.

15. S.C. Singhal, Corrosion-Resistant Structural Ceramic Materials for Gas Turbines, Gas Turbine Materials in the Marine Environment 1974, MCIC-75-27, (J.W. Fairbanks and I. Machlin, eds.) Metals and Ceramics Information Center, Battelle Labs, Columbus, OH, 1974, p. 311.

16. R.H. Arendt and M.J. Curran, Corrosion of Dense Silicon Carbide in Basic Molten Salt Solutions, Metal-Slag-Gas Reactions and Processes, (Z.A. Foroulis and W.W. Smeltzer, eds.) The Electrochemical Society, Pennington, NJ, 1975, p. 636.

17. J. Schlichting, "Heisskorrosionsverhalten von SiC und Si_3N_4 im Brennergas," Werkst. Korros., 26[10]: 753 (1975).

18. J. Schlichting, Oxidation and Hot Corrosion Behavior of Si_3N_4 and SiAlON, Nitrogen Ceramics, (F.L. Riley, ed.) Noordhoff, Leyden, 1977, p. 627.

19. J. Schlichting, "Oxidation Kinetic of Silicon Ceramic from the Point of Refractory Materials Resistant Against Hot Corrosion," Rev. Int. Hautes Temp. Refract., 16: 67 (1979).

20. J. Schlichting, New Results on Hot Corrosion of Silicon Ceramics, High Temperature Corrosion of Metals and Alloys, Japan Institute of Metals, Tokyo, Japan, 1983, p. 607.

21. D.W. McKee and D. Chatterji, "Corrosion of Silicon
    Carbide in Gases and Alkaline Melts," J. Am. Ceram.
    Soc., 59[9-10]: 441 (1976).

22. R.E. Tressler, M.D. Meiser, and T. Yonushonis, "Molten
    Salt Corrosion of SiC and Si_3N_4 Ceramics," J. Am. Ceram.
    Soc., 59[5-6]: 278 (1976).

23. W.C. Bourne and R.E. Tressler, Alteration of Flaw Sizes
    and KIc's of Si_3N_4 Ceramics by Molten Salt Exposure,
    Fracture Mechanics of Ceramics, Vol. 3, (R.C. Bradt,
    D.P.H. Hasselman, and F.F. Lange, eds.) Plenum Press,
    New York, 1978, p. 113.

24. W.C. Bourne and R.E. Tressler, "Molten Salt Degradation
    of Si_3N_4 Ceramics," Am. Ceram. Soc. Bull., 59[4]: 443
    (1980).

25. E. Erdoes and H. Altorfer, Corrosion Behavior of
    Hot-Pressed and Reaction-Bonded Silicon Nitride in
    Condensed Phases, Materials and Coatings to Resist High
    Temperature Corrosion, (D.R. Holmes and A. Rahmel, eds.)
    Elsevier Applied Science Publishers, London, 1977, p.
    161.

26. C.T. Sims and J.E. Palko, Surface Stability of Ceramics
    Applied to Energy Conversion Systems, Proceedings of the
    Workshop on Ceramics for Advanced Heat Engines,
    CONF-770110, Dept. of Energy, Washington, D.C., 1977,
    p. 287.

27. J.E. Palko, "A Review of Oxidation and Hot Corrosion of
    Silicon Based Ceramics," Report 77-GTD-55, General
    Electric, Schenectady, NY, 1977.

28. M.I. Mayer and F.L. Riley, "Sodium-Assisted Oxidation of
    Reaction-Bonded Silicon Nitride," J. Mater. Sci., 13:
    1319 (1978).

29. M.I. Mayer and F.L. Riley, "Sodium Ion Assisted Oxidation
    of Reaction-Bonded Silicon Nitride," Proc. Br. Ceram.
    Soc., 26: 251 (1978).

30. M. Levy and J.J. Falco, "Hot Corrosion of Reaction-
    Bonded Si_3N_4," Am. Ceram. Soc. Bull., 57[4]: 457 (1978).

31. D.W. Richerson and T.M. Yonushonis, Environmental Effects on the Strength of Silicon-Nitride Materials, Proceedings of the DARPA/NAVSEA Ceramic Gas Turbine Demonstration Engine Program Review, MCIC-78-36, (J.W. Fairbanks and R.W. Rice, eds.) Metals and Ceramics Information Center, Battelle Labs, Columbus, OH, 1977, p. 247.

32. D.W. Richerson and K.M. Johansen, "Ceramic Gas Turbine Engine Demonstration Program," REPT-21-4410, Garrett Turbine Engine Co., Phoenix, AZ, 1982. (Avail. NTIS, AD-A117088).

33. S. Brooks and D.B. Meadowcroft, "The Corrosion of Silicon-Based Ceramics in Residual Fuel-Oil-Fired Environment," Proc. Br. Ceram. Soc., 26: 237 (1978).

34. R.H. Barkalow and F.S. Pettit, Evaluation of Hot Corrosion Resistance of Candidate Ceramic Coatings for Industrial/Utility Gas Turbines, 4th Annual Conference on Materials for Coal Conversion and Utilization, CONF-791014, Dept. of Energy, Washington, D.C., 1979, p. II.58.

35. R.N. Katz, "Corrosion/Erosion Behavior of Silicon Nitride and Silicon Carbide Ceramics: Gas Turbine Experience," AMMRC-MS-79-2, Army Materials and Mechanics Research Center, Watertown, MA, 1979. (Avail. NTIS, AD-A076382).

36. P.L. Cavallotti, U. Ducati, and P.C. Martinengo, Oxidation and Hot Corrosion Behavior of Sintered Nitrogen Ceramics, Ceramics for Turbine Engine Applications, AGARD-CP-276, AGARD, Neuilly-Sur-Seine, France, 1979. (Avail. NTIS, AD-A087594).

37. D.E. Schwab and D.M. Kotchick, "High Temperature Strength of Sintered α-SiC in Salt and Oxidizing Environments," Am. Ceram. Soc. Bull., 59[8]: 805 (1980).

38. J.C. Napier, "Manufacturing Methods for Ceramic Nozzle Section for Gas Powered APU'S," Report SR84-R-4692-64, Solar Turbines Incorporated, San Diego, CA, May 7, 1984.

39. J.R. Blachere and F.S. Pettit, "High-Temperature Corrosion of Ceramics," DOE/ER/10915-3, 1984.

40. J.R. Blachere and F.S. Pettit, "High-Temperature Corrosion of Ceramics," DOE/ER/10915-4, 1984.

41. J.R. Blachere and F.S. Pettit, "High-Temperature Corrosion of Ceramics," Progress Report DOE/ER/45117-1, 1985.

42. W.L. Fielder, "Oxidation and Hot Corrosion of Hot-Pressed Si_3N_4 at 1000°C," NASA TM-86977, 1985.

43. G.A. Gogotsi, Yu. G. Gogotsi, V.P. Zavada, and S.I. Sopenko, "Action of Salts on the Strength and Crack Resistance of Silicon Nitride Ceramics," Strength Mater. (Engl. Transl.), 16[11]: 1515 (1984).

44. G.A. Gogotsi, V.P. Zavada, and Yu. G. Gogotsi, "Strength Degradation of Si_3N_4 - SiC-Based Ceramics in Salt Environments," Ceram. Int., 12[4]: 203 (1986).

45. N.S. Jacobson and J.L. Smialek, "Hot Corrosion of Sintered α-SiC at 1000°C," J. Am. Ceram. Soc., 68[8]: 432 (1985).

46. N.S. Jacobson, "Kinetics and Mechanism of Corrosion of SiC by Molten Salts," J. Am. Ceram. Soc., 69[1]: 74 (1986).

47. N.S. Jacobson, C.A. Stearns, and J.L. Smialek, "Burner Rig Corrosion of SiC at 1000°C," Adv. Ceram. Mater., 1[2]: 154 (1986).

48. R. Browning, J. Smialek, and N. Jacobson, "Scanning Auger Microscopy of Corroded SiC," J. Mater. Sci. Lett., 5: 1122 (1986).

49. J.L. Smialek and N.S. Jacobson, "Mechanism of Strength Degradation for Hot Corrosion of α-SiC," J. Am. Ceram. Soc., 69[10]: 741 (1986).

50. N.S. Jacobson and J.L. Smialek, "Corrosion Pitting of SiC by Molten Salts," J. Electrochem. Soc., 133[12]: 2615 (1986).

51. D.S. Fox and N.S. Jacobson, "Molten-Salt Corrosion of Silicon Nitride: I, Sodium Carbonate," J. Am. Ceram. Soc., 71[2]: 128 (1988).

52. N.S. Jacobson and D.S. Fox, "Molten-Salt Corrosion of Silicon Nitride: II, Sodium Sulfate," J. Am. Ceram. Soc., 71[2]: 139 (1988).

38

I

53. N.S. Jacobson, "Sodium Sulfate: Deposition and Dissolution of Silica," to appear in Oxid. Met., (1988).

54. D.S. Fox and J.L. Smialek, "Burner Rig Hot Corrosion of Ceramic Engine Materials," submitted to Adv. Ceram. Mater., (1988).

55. D.S. Fox and N.S. Jacobson, "The Effect of Hot Corrosion on the Microstructure and Strength of Silicon Nitride", in preparation.

56. N.J. Tighe, J. Sun, and R.M. Hu, "Corrosion Reactions in SiC Ceramics," Ceram. Eng. Sci. Proc., 8[7-8]: 805 (1987).

57. C.H. Henager, Jr. and R.H. Jones, "Environmental Effects on Slow Crack Growth in Silicon Nitride," Ceram. Eng. Sci. Proc., 9[7-8]: (1988).

58. R. Nagarajan, "CVD Processes Leading to the Formation and Dissolution of Ceramic Coatings on Combustion Turbine Airfoils," Heat Transfer--Houston 1988, (S.B. Yilmaz, ed.) AIChE Symposium Series, 84[263]: 86 (1988).

59. M.K. Ferber and V.J. Tennery, "Evaluation of Tubular Ceramic Heat Exchanger Materials in Acidic Coal Ash from Coal-Oil-Mixture Combustion," ORNL/TM-7958, 1981.

60. M.K. Ferber and V.J. Tennery, "Evaluation of Tubular Ceramic Heat-Exchanger Materials in Basic Coal Ash from Coal-Oil-Mixture Combustion," ORNL/TM-8385, 1982.

61. M.K. Ferber, V.J. Tennery, and J.F. Willmering, "Exposure of Tubular Ceramic Heat Exchanger Materials to Refractory Coal Ash from Coal-Oil-Mixture Combustion," ORNL/TM-9052, 1984.

62. P.F. Becher, "Strength Degradation in SiC and Si_3N_4 Ceramics by Exposure to Coal Slags at High Temperatures," J. Mater. Sci., 19: 2805 (1984).

63. M.K. Ferber, J. Ogle, V.J. Tennery, and T. Henson, "Characterization of Corrosion Mechanisms Occurring in a Sintered SiC Exposed to Basic Coal Slags," J. Am. Ceram. Soc., 68[4]: 191 (1985).

64. M.K. Ferber, J. Ogle, and P.F. Becher, "Effect of Oxidizing and Coal-Slag Environments upon the Time-Dependent Strength Behaviour of a Sintered SiC," J. Mater. Sci., 21: 2678 (1986).

65. T.E. Easler and R.B. Poeppel, "Corrosion of Ceramics in Heat Exchanger Applications," High Temperature Corrosion in Energy Systems, (M.F. Rothman, ed.), Metallurgical Society of AIME, Warrendale, PA, 1984, p.   .

66. T.E. Easler, "Corrosion Behavior and Mechanical Properties of Silicon Carbide Exposed to a Coal Gasification Environment," ANL/FE-84-21, Argonne National Laboratory, (1985).

67. T.E. Easler, "Effects of Coal Gasification Environments on Corrosion Behavior and Mechanical Properties of Siliconized Silicon Carbide," ANL/FE-85-6, Argonne National Laboratory, 1985.

68. T.E. Easler, "Comparison of Results of 200- and 500-h Exposures of Silicon Carbide to a Slagging Coal Gasification Environment," ANL/FE-85-13, Argonne National Laboratory, 1986.

69. E. Buchner and O. Rubisch, Corrosion Behavior of Silicon Carbide Heating Elements, Silicon Carbide - 1973, (R.C. Marshall, J.W. Faust Jr., and C.E. Ryan, eds.) University of South Carolina Press, Columbia, SC, 1974, p. 428.

70. G.W. Weber and V.J. Tennery, "Materials Analyses of Ceramics for Glass Furnace Recuperators," ORNL/TM-6970, (1979).

71. G.C. Wei and C.L. White, "High Temperature Behavior of Pressureless-Sintered SiC in a Steel Soaking Pit Environment," Am. Ceram. Soc. Bull., 63[7]: 890 (1984).

72. J.I. Federer, T.N. Tiegs, D.M. Kotchick, and D. Petrak, "Analysis of Candidate Silicon Carbide Recuperator Materials Exposed to Industrial Furnace Environments," ORNL/TM-9677, (1985).

73. J.I. Federer and P.J. Jones, "Oxidation/Corrosion of Metallic and Ceramic Materials in an Aluminum Remelt Furnace," ORNL/TM-9741, 1985.

74. J.I. Federer, J.M. Robbins, P.J. Jones, and C. Hamby, Jr. "Corrosion of SiC Ceramics in Synthetic Combustion Atmospheres Containing Halides," ORNL-6258, 1985.

75. J.I. Federer, "Corrosion of SiC Ceramics by Na_2SO_4," Adv. Ceram. Mater., 3[1]: 56 (1988).

76. J.I. Federer, "Stress-Corrosion of SiC in an Oxidizing Atmosphere Containing NaCl," Adv. Ceram. Mater., 3[3]: 293 (1988).

77. J.I. Federer, "Corrosion of Materials by High-Temperature Industrial Combustion Environments – A Summary," ORNL/TM-9903, (1986).

78. J. Van Ackeren and T. Stillwagon, Corrosion of Silicon Carbide Tubes in Industrial Flue Gas Streams, Corrosion of Ceramic Materials Workshop: Proceedings, (B.K. Kennedy, ed.) Center for Advanced Materials, Pennsylvania State University, University Park, PA, 1987, p. 43.

79. J.W. Cree and M.F. Amateau, "Mechanical Behavior of SiC Exposed to Molten Lithium and Lithium Salts," Ceram. Eng. Sci. Proc., 8[7-8]: 812 (1987).

80. T. Sato, Y. Kanno, and M. Shimada, "Corrosion of SiC, Si_3N_4, and AlN in Molten K_2SO_4–K_2CO_3 Salts," Int. J. High Technol. Ceram., 2[4]: 279 (1986).

81. T. Sato, Y. Kanno, T. Endo, and M. Shimada, "Corrosion of Si_3N_4 in Molten Alkali Sulfate and Carbonate," Adv. Ceram. Mater., 2[3A]: 228 (1987).

82. M. Shimada, T. Sato, and T. Endo, High Temperature Corrosion and Degradation in Strength of Silicon Nitride Based Ceramics by Alkali Sulfates and Carbonates Melts, High Temperature Materials Chemistry IV, (Z.A. Munir, D. Cubicciotti, and H. Tagawa, eds.) The Electrochemical Society, Pennington, NJ, 1987.

83. T. Sato, Y. Koike, T. Endo, and M. Shimada, "Corrosion and Strength Degradation of Si_3N_4 and Sialons in K_2CO_3 and K_2SO_4 Melts," J. Mater. Sci., 23: 1405 (1988).

84. K. Tajiri, T. Nishio, T. Asahina, and M. Kosaka, Corrosion of Hot-Pressed Silicon Nitride in Alkali Carbonate Melts, Joint International Symposium on Molten Salts, (G. Mamantov, M. Blander, C. Hussey, C. Mamantov, M.L. Saboungi, and J. Wilkes, eds.) The Electrochemical Society, Pennington, NJ, 1987, p. 717.

85. S. Gordon and B.J. McBride, "Computer Program for Calculation of Complex Chemical Equilibrium Compositions, Rocket Performance, Incident and Reflected Shocks, and Chapman-Jouget Detonations", NASA SP-273, 1976.

86. W.D. Kingery, H.K. Bowen, and D.R. Uhlmann, Introduction to Ceramics, Wiley, New York, 1976, p. 359.

87. A.D. Pelton, C.W. Bale, and W.T. Thompson, "FACT (Facility for the Analysis of Chemical Thermodynamics) – A Computerized Canadian Thermodynamic Data Treatment Center," Applications of Phase Diagrams in Metallurgy and Ceramics, NBS-SP-496, Vol. 2, National Bureau of Standards, Gaithersburg, MD, 1978, p. 1077.

88. R. Browning, J.L. Smialek, and N.S. Jacobson, "Multi-element Mapping of α-SiC by Scanning Auger Microscopy," Adv. Ceram. Mater., 2[4]: 773 (1987).

89. S.C. Singhal and F.F. Lange, "Effect of Alumina Content on the Oxidation of Hot-Pressed Silicon Carbide", J. Am. Ceram. Soc., 58[9-10]: 433 (1975).

90. D. Cubicciotti and K.H. Lau, "Kinetics of Oxidation of Yttria Hot-Pressed Silicon Nitride", J. Electrochem. Soc., 126[10]: 1723 (1979).

91. J.R. Price, R.E. Gildersleeve, M. Van Roode, and C.E. Smeltzer, "A New Ceramic Recuperation Technology for Use in Corrosive Environments", Corrosion of Ceramic Materials Workshop: Proceedings, (B.K. Kennedy, ed.) Center for Advanced Materials, Pennsylvania State University, University Park, PA, 1987, p. 81.

TABLE I. — CORROSIVE APPLICATIONS FOR CERAMICS

Application	Temperatures	Pressures atm,	Atmosphere	Deposit
Heat engines	900 to 1400 °C	1 to 50	Oxidizing	Na_2SO_4, $Na_2V_xO_y$
Coal combustion	1200 to 1400 °C	1 to 10	Reducing	Acidic or basic coal slags
Industrial furnaces	1000 to 1600 °C	~1	Oxidizing, reducing	NaCl, NaF, Na_2SO_4, Transition metal oxides
Magneto-hydrodynamics	1000 to 1400 °C	1 to 10	Oxidizing, reducing	K_2CO_3, K_2SO_4
Fuel cells	800 to 1000 °C	~1	Oxidizing	Alkali carbonates

TABLE II.

(a) Types of SiC

Designation	Material	Additives, impurities	Type, manufacturer
SCSC	Single crystal SiC	Fe	————————————
CVDSC	Chemically vapor deposited SiC	———————	————————————
RSC	Recrystallized SiC	~18 percent porous	NC400, Norton Co, Worcestor, MA
RBSC	Reaction bonded SiC Siliconized SiC	Si	Various types e.g., Sohio KX01 Standard Oil Engineered Materials Co. Niagara Falls, NY
HPSC	Hot pressed SiC	Al_2O_3	NC203, Norton Corp, Worcestor, MA
SSC (Al, C)	Sintered SiC	Al, C	————————————
SASC (B, C)	Sintered α-SiC	B, C	Sohio Hexoloy Standard Oil Engineered Materials Co. Niagara Falls, NY
SBSC (B, C)	Sintered β-SiC	B, C	General Electric
NSSC (B, C)	Sintered SiC	B, C	NGK Spark Plug Co., Ltd. Japan

TABLE II. – Concluded.

(b) Types of Si_3N_4

Designation	Material	Additives, impurities	Type, manufacturer
CVDSN	Chemically vapor depos- ited Si_3N_4	------------	------------------------
RBSN	Reaction bonded Si_3N_4	Si	------------------------
HIP RBSN	Hot isostatically pressed reaction bonded Si_3N_4	Si	See reference 7
HPSN (MgO)	Hot pressed Si_3N_4	MgO	NC132, Norton Corp, Worcestor, MA
HPSN (Y_2O_3)	Hot pressed Si_3N_4	Y_2O_3, WC	NCX-34, Norton Corp, Worcestor, MA
SSN (Al_2O_3, Y_2O_3)	Sintered Si_3N_4	Al_2O_3, Y_2O_3	AY-6, GTE Products Corp, Towanda, PA
SSN (Y_2O_3)	Sintered Si_3N_4	Y_2O_3	PY-6, GTE Products Corp, Towanda, PA
HPSN (Al_2O_3, Y_2O_3)	Hot pressed Si_3N_4	Al_2O_3, Y_2O_3	Toshiba Ceramic Co., Ltd. Tokyo, Japan
NSSN (Al_2O_3, Y_2O_3)	Sintered Si_3N_4	Al_2O_3, Y_2O_3	NGK Spark Plug Co., Ltd. Japan

I

TABLE III. – SURVEY OF CORROSION STUDIES

(a) Etching studies

Date	Reference	Materials	Corrodents	Technique	Observations
1952	(8) Horn	SCSC	Na_2CO_3 1000 °C	Crucible	Pitting at dislocation sites
1959	(9) Faust		Basic salts		Pitting
1960	(10) Amelinckx et al.		Na_2CO_3 1000 °C		Pitting at dislocation sites
1963	(11) Gabor, Stickler		PbO, $PbO-PbF_2$		Pitting
1965	(12) Gabor, Jennings		$NaF-Na_2SO_4$		Pitting at dislocation and impurity sites. Etch rate highly temperature dependent At 1050 °C ~130 μ/min
1974	(13) Faust, Liaw		Basic oxides		Review of etching studies

(b) Heat engines

Date	Reference	Materials	Corrodents	Technique	Observations
1972–74	(14, 15) Singhal	HPSC (Al_2O_3) HPSN (MgO)	Na_2SO_4, V_2O_5 1100 °C	Burner	Limited deposition and corrosion
1975	(16) Arendt, Curran	HPSC	$CaF_2-BaF_2-CaSO_4$ SrF_2MgSO_4 ≤1100 °C	Crucible	Severe etching by basic salts. Arrhenius behavior
1975–83	(17 to 20) Schlichting	RBSC HPSC SSC (Al) SSC (B) RBSN HPSN (Y_2O_3) HPSN (MgO)	NaCl, Na_2CO_3 Na_2SO_4, V_2O_5 1000 to 1200 °C	Crucible, Burner	Formation of liquid $Na_2O \cdot x(SiO_2)$ with Na_2CO_3 and Na_2SO_4 leads to rapid corrosion
1976	(21) McKee, Chatterji	SBSC (B, C)	Na_2SO_4 Na_2SO_4 + C Na_2CO_3	Crucible, Thin film	Limited corrosion in acidic melts. Dissolution in basic melts. Active oxidation in C containing melts due to low $P(O_2)$

TABLE III. – Continued.

(b) Heat engines

Date	Reference	Materials	Corrodents	Technique	Observations
1976–80	(22 to 24) Tressler et al.	RBSC HPSC (Al_2O_3) RBSN HPSN (MgO)	Na_2SO_4 (+NaCl)	Crucible	Rapid consumption in Na_2SO_4 SiC corrodes faster than Si_3N_4 Na,S,Cl grain boundary penetration Severe (~50 percent) strength degradation
1977	(25) Erdos, Altorfer	HPSN RBSN	Na_2SO_4 (+NaCl + V_2O_5) (+NaCl + Li_2O) (+MgSO_4 + CaSO_4$)	Crucible, Burner	Severe corrosion with basic salts
1977	(26, 27) Palko, Sims	HPSC HPSN SSC	Na_2SO_4, V_2O_5 800 to 1100 °C	Burner	Limited corrodent penetration ~25 μm/1000 hr
1978	(28, 29) Mayer, Riley	RBSN	Na_2CO_3, Na_2SO_4, NaCl 800 to 1300 °C	Film, Salt vapor	Na_2CO_3: Initial rapid $Na_2O \cdot x(SiO_2)$ formation, reaction slows with SiO_2 formation Na_2SO_4, NaCl vapors: $Na_2O \cdot x(SiO_2)$ formation
1978	(30) Levy, Falco	RBSN	Na_2CO_3, Na_2SO_4 1093 °C	Film	Friable corrosion products Extensive surface roughening
1978–81	(31, 32) Richerson et al.	HPSN (MgO) RBSN	Na_2SO_4 1075, 1125 °C	Burner	Glassy corrosion products Strength degradation
1978	(33) Brooks, Meadowcroft	RBSC RBSN HPSN	Na_2SO_4, V_2O_5 900 to 1400 °C	Crucible, Burner	Extensive deposition and corrosion $Na_2O \cdot x(SiO_2)$ formation
1979	(34) Barkalow, Pettit	Si_3N_4	Na_2SO_4 – 982 °C	Film	More attack with lower $P(SO_3)$ – basic Na_2SO_4
1979	(35) Katz	Si_3N_4, SiC	Na_2SO_4, V_2O_5	Burner	Review – points out need for more data

TABLE III. – Continued.

(b) Heat engines

Date	Reference	Materials	Corrodents	Technique	Observations
1979	(36) Cavallotti	HPSN (Y_2O_3, MgO) RBSN (Fe_2O_3, MgO) RBSSN (Y_2O_3, MgO) SSN (Y_2O_3, MgO)	NaCl, Na_2SO_4	Film	Formation of $Na_2O \cdot x(SiO_2)$ RBSN corrodes the most
1980	(37) Schwab, Kotchick	SASC (B, C)	Sea salt 1200 to 1400 °C	Film	Enhanced slow crack growth with salt deposit
1982	(38) Napier	RBSC HPSN	NaCl + Na_2SO_4 $MgSO_4$ + Na_2SO_4 V_2O_5 + Na_2CO_3 593 °C, 871 °C	Film	No strength decrease for RBSC ~50 percent strength decrease for HP Si_3N_4 + (V_2O_5 + Na_2CO_3)
1984-85	(39 to 41) Blachere, Pettit	SCSC CVDSC HPSC (Al_2O_3) CVDSN HPSN (Y_2O_3)	Na_2SO_4 1000 °C	Film	Na_2SO_4/O_2 – Dissolution of SiO_2 layer Na_2SO_4/SO_3 – Spherolitic devitrification of SiO_2 layer
1985	(42) Fielder	HPSN (Y_2O_3)	Na_2SO_4	Film	Incubation period, massive liquid $Na_2O \cdot x(SiO_2)$ scales with bubbles, SO_2 evolution
1986	(43, 44) Gogotsi, et al.	Si_3N_4-SiC-MgO	NaCl, Sea salt, Na_2SO_4	Crucible, Film	Na_2SO_4 – Most corrosive salt Strength and K_{IC} degradation with all salts
1986-88	(45 to 55) Jacobson, Smialek, Fox	SCSC CVDSC SASC (B, C) HPSC (Al_2O_3) CVDSN HIP RBSN SSN (Y_2O_3, Al_2O_3) SSN (Y_2O_3) HPSN (MgO)	Na_2SO_4, Na_2CO_3 1000 °C	Film, Burner rig	Severe attach by basic molten salts due to coupled oxidation-dissolution Carbon can drive Na_2SO_4 basic Severe pitting in SiC leads to strength reduction; grain boundary attack in Si_3N_4

TABLE III. - Continued.

(b) Heat engines

Date	Reference	Materials	Corrodents	Technique	Observations
1987	(56) Tighe et al.	SASC (B, C)	Na_2CO_3	Thin film	Dissolution at grain boundaries and intergranular faults
1988	(57) Henninger, Jones	HPSN (Y_2O_3)	Na_2SO_4	Film	Enhanced slow crack growth, due to SiO_2 dissolution
1988	(58) Nagarajan	SiC	Na_2SO_4	---------	Theoretical discussion on deposition of Na_2SO_4 and dissolution of SiO_2

(c) Coal combustion

Date	Reference	Materials	Corrodents	Technique	Observations
1981–86	(59 to 64) Ferber, Becher et al.	CVDSC RBSC SASC (B, C)	Acidic coal slag Basic coal slag	Burner, Film	Extensive surface recession with basic slags Pitting due to formation of (Fe, Ni) silicide leads to strength reduction Strength degradation-material and slag dependent
1984–85	(65 to 68) Easler, Poeppel	RBSC SASC (B, C)	Acidic coal slag Basic coal slag	Film	More attack and strength reduction from basic slag Penetration of Fe along grain boundaries Formation of SiO_2 healing layer between slag and SiC

48

TABLE III. – Continued.

(d) Industrial furnaces

Date	Reference	Materials	Corrodents	Technique	Observations
1974	(69) Buchner, Rubisch	RBSC	Na_2CO_3 ≤ 900 °C	Crucible	Complete dissolution
1979	(70) Weber, Tennery	CVDSC RSC RBSC SASC (B, C)	Glass melting furnace 1150 to 1550 °C	Actual Furnace	Extensive corrosion when alkali salts deposited at lower temperatures
1984	(71) Wei, White	SASC (B, C)	Steel soaking pit 1250 °C	Actual Furnace	Slag deposit, but no appreciable degradation
1985	(72 to 73) Federer et al.	CVDSC RSC RBSC SASC (B, C)	Al remelt furnace Forge furnace Steel reheat furnace Steel soaking pits	Actual Furnace	Degradation in Al remelt furnace and in one steel soaking pit
1985–88	(74 to 76) Federer et al.	RBSC SASC (B, C) 1200 °C	NaCl NaF 1200 °C	Vapor	Na_2O formed from NaCl leads to $Na_2O \cdot x(SiO_2)$ Surface recession Early failure under stress
1986	(77) Federer	Various SiC, Si_3N_4	Industrial furnaces Coal combustors	---------	Summary of corrosion tests in industrial furnaces and coal combustion
1987	(78) Van Ackeren	RBSC SASC (B, C)	Steel soaking pit Forging furnace Al Remelt – continuous fluxing Al Remelt – non-fluxing	Actual Furnace	Most corrosion in continuous fluxing furnace (contains salts)
1987	(79) Cree, Amateau	SASC (B, C)	LiF, LiCl, LiS, $LiSO_4$, Li 200 to 1000 °C	Film	Scale dissolution, Li penetration

TABLE III. – Concluded.

(e) MHD, Fuel cells

Date	Reference	Materials	Corrodents	Technique	Observations
1986–87	(80 to 83) Shimada et al.	NSSC NSSN (Y_2O_3, Al_2O_3)	K_2SO_4-K_2CO_3	Crucible	Dissolution of SiC, Si_3N_4 20 to 30 percent strength degradation AlN shows good corrsion resistance
1987	(84) Tajiri et al.	HPSN (Y_2O_3, Al_2O_3)	Li_2CO_3, Na_2CO_3 K_2CO_3	Crucible	Corrosion rates $Li_2CO_3 > Na_2CO_3$ $> K_2CO_3$

TABLE IV. - DEW POINTS FOR Na$_2$SO$_4$ DEPOSITION

[Temperatures in degrees Celsius, salt concentrations in parts per million. Deposit is liquid unless noted.]

Percent S in fuel	P, atm	0.001 Na	0.01 Na	0.1 Na	1.0 Na	10 Na
0.5	1	[a]747	[a]814	887	961	1025
	5	[a]793	[a]867	953	1039	1113
	10	[a]814	892	984	1075	1155
	50	[a]867	958	1062	1166	1260
	100	893	989	1098	1208	1310
0.05	1	[a]746	[a]810	[a]876	937	991
	5	[a]792	[a]862	940	1011	1072
	10	[a]813	887	969	1045	1111
	50	[a]865	951	1042	1130	1207
	100	889	980	1076	1169	1252

[a]Solid.

TABLE V. - TYPICAL COAL SLAG COMPOSITION[a]

	Acidic	Basic
SiO$_2$	54	46
Fe$_2$O$_3$	21	11
Al$_2$O$_3$	19	14
CaO	0.1	19
MgO	0.9	7
Na$_2$O	0.6	1.1
K$_2$O	1.7	0.5
TiO$_2$	1.3	0.3
Ratio basic oxides to acidic oxides[b]	0.29	1.14

[a]From reference 59.
[b][Σ wt % (Fe$_2$O$_3$ + CaO + MgO + Na$_2$O + K$_2$O)/Σ wt % (SiO$_2$ + Al$_2$O$_3$ + TiO$_2$.]

TABLE VI. - CHEMICAL ANALYSIS RESULTS

[SiC, Si$_3$N$_4$ + Na$_2$SO$_4$/.01SO$_3$-O$_2$ - 48 hr, 1000 °C.]

Material	Water soluble			Water insoluble SiO$_2$, mg/cm^2
	Na$_2$SO$_4$, mg/cm^2	Na$_2$O·x (SiO$_2$)		
		mg/cm^2	x	
SCSC	1.64±0.86	<0.01	-------	1.82±0.96
HPSC	2.01±0.03	<0.01	-------	0.39±0.02
SASC (B, C)	0.49±0.06	0.97±0.28	1.6±0.9	10.50±0.66
SSN (Y$_2$O$_3$, Al$_2$O$_3$)	0.23±0.11	---------	-------	1.3±0.2

TABLE VII. - PIT SIZE DISTRIBUTIONS FOR CORRODED SASC (B, C)--NUMBER OF PITS PER 1 mm^2 AREA

	Diameter < 10 μm	10 μm < diameter < 20 μm	Diameter > 20 μm
Na$_2$SO$_4$/SO$_3$	1,880	620	90
Na$_2$CO$_3$/CO$_2$	2,280	30	4
Na$_2$SO$_4$/AIR	17,280	120	6

(a)   (b)
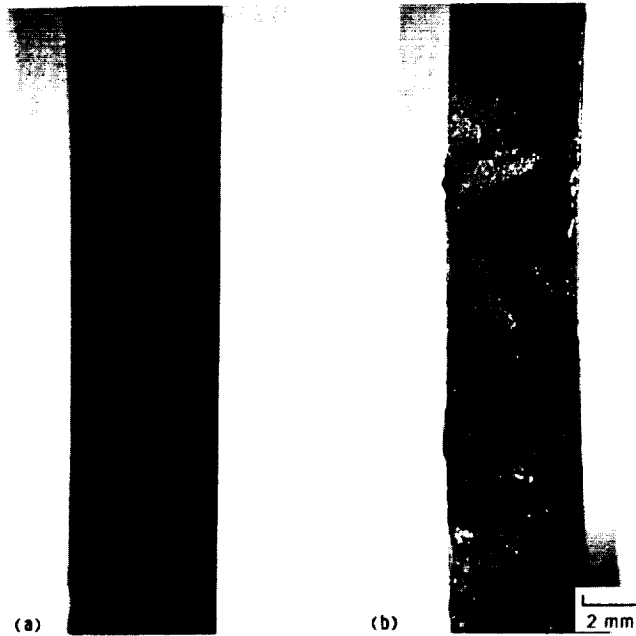
(a) 46 HR WITH NO Na.   (b) 13.5 HR WITH 4 PPM Na.
LEADING EDGE IS ON LEFT.

FIGURE 1. - OPTICAL MICROGRAPHS OF SASC (B,C) TREATED IN THE BURNER
RIG AT 1000 °C WITH JET A FUEL.
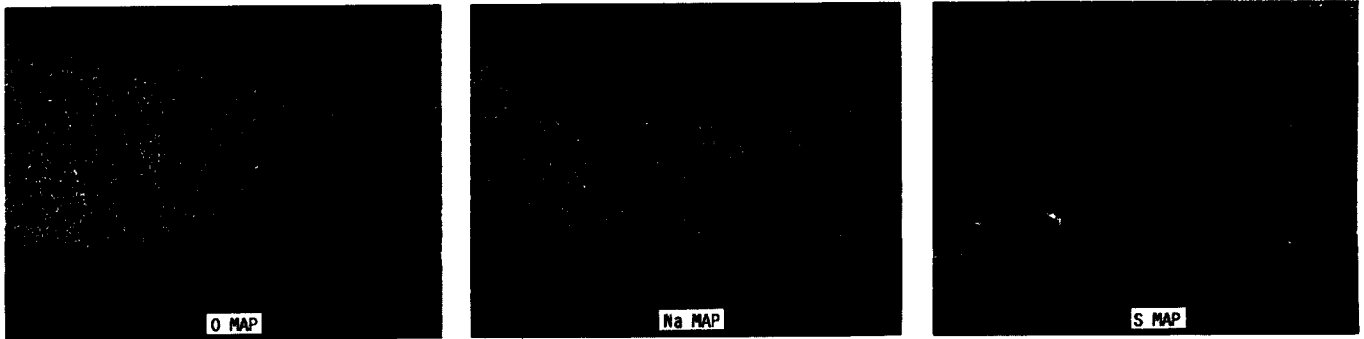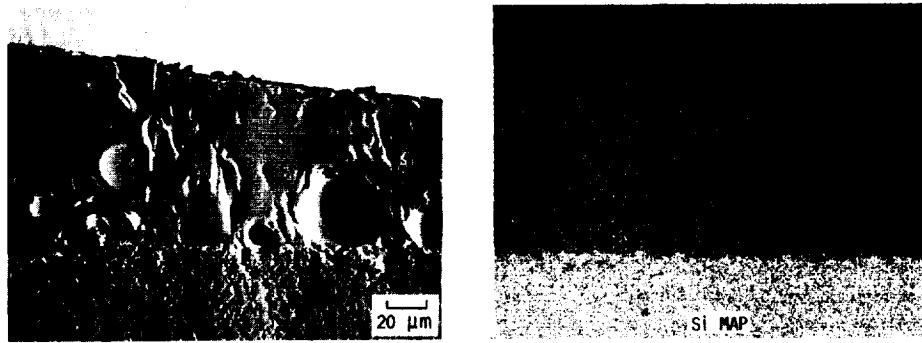
FIGURE 2. - ELECTRON MICROPROBE ANALYSIS OF A POLISHED CROSS SECTION OF GLASSY PRODUCTS ON SASC (B,C) FORMED BY BURNER RIG CORROSION AT
1000 °C WITH JET A FUEL FOR 13.5 HR WITH 4 PPM Na.

51
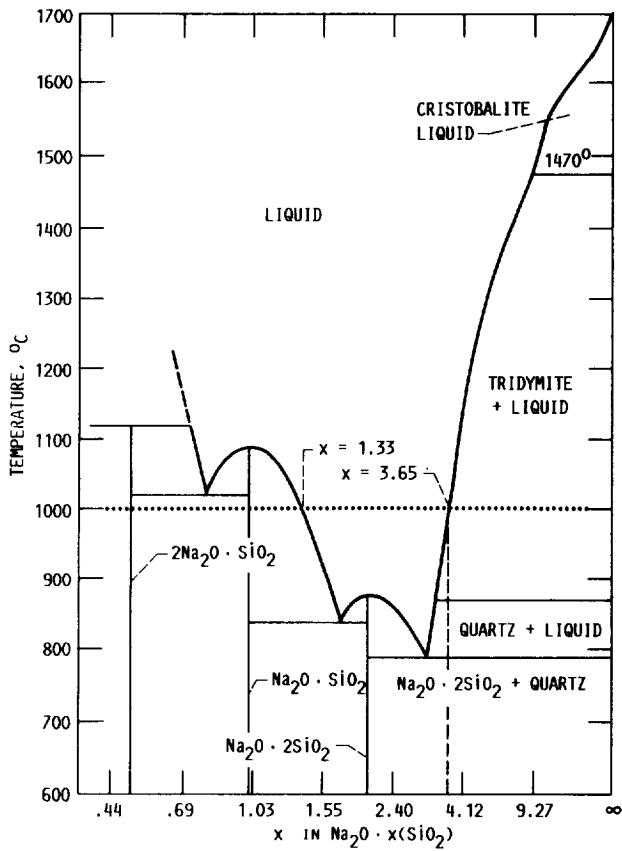
FIGURE 3. - Na_2O - SiO_2 PHASE DIAGRAM.
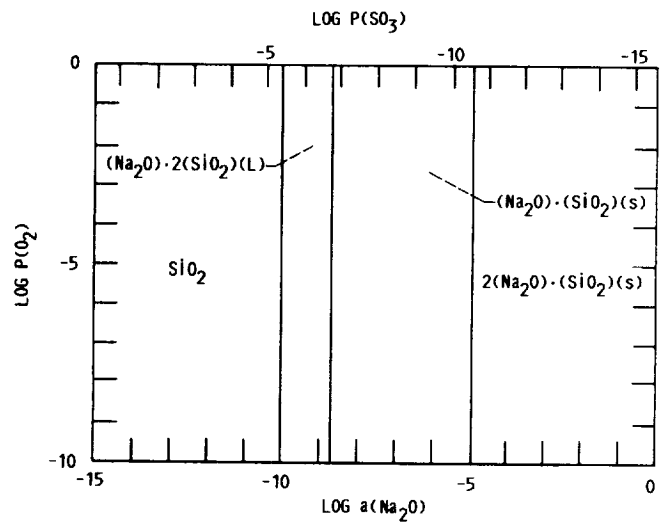
FIGURE 4. - Si-O-Na STABILITY DIAGRAM.
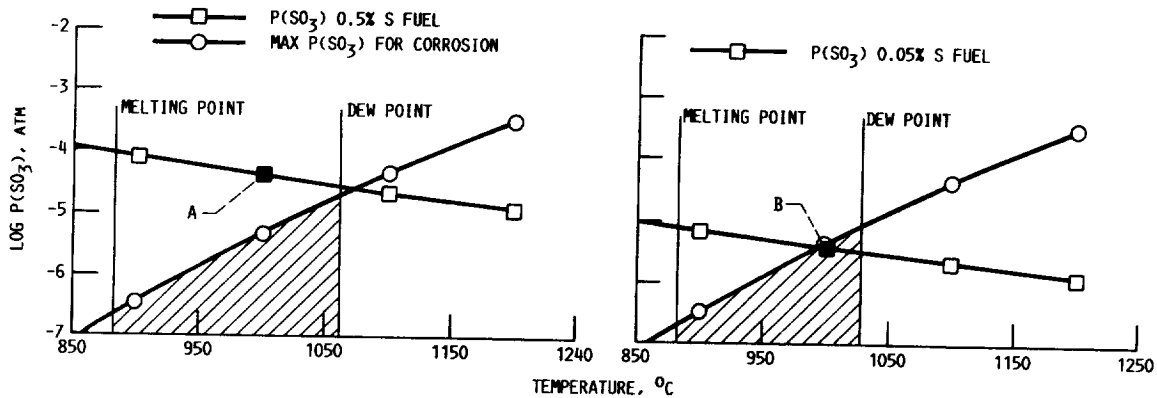
(a) 0.5% S FUEL, 2 PPM Na, 0.025 FUEL-TO-AIR RATIO, 1000 °C.

(b) 0.05% S FUEL, 2 PPM Na, 0.025 FUEL-TO-AIR RATIO, 1000 °C.

FIGURE 5. - CALCULATED CORROSION REGIMES FOR SiO_2.

52
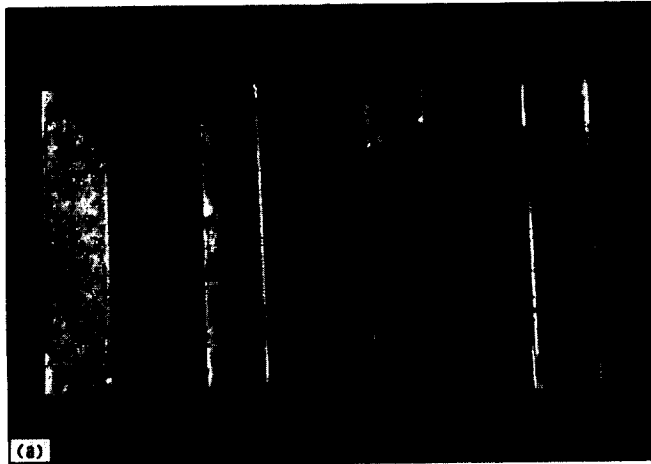
(a) NUMBER 2 DIESEL FUEL (0.5% S), 5 HR.

(b) JET A FUEL (0.05% S), 1 HR.

FIGURE 6. - SiO_2 COUPONS TREATED IN THE BURNER RIG, 2 PPM Na, 1000 °C.


```
                    ┌─────────────┐
                    │  CORRODED   │
                    │  SAMPLE     │
                    └─────────────┘
                           │
                           ▼
      ┌──────────────────┐   SOLUTION
      │ 2 HR IN HOT      │──────────────►  Na - FROM Na₂SO₄, Na₂O · x(SiO₂)
      │ DEIONIZED WATER  │                 Si - FROM Na₂O · x(SiO₂)
      └──────────────────┘                 SO₄= - FROM Na₂SO₄
                           │
                           ▼
      ┌──────────────────┐   SOLUTION
      │ 2 HR IN HOT 10% HF│─────────────►  Si - FROM SiO₂
      │ DEIONIZED WATER  │                 Na - IN SiO₂
      └──────────────────┘
```

Na - FROM Na_2SO_4, $Na_2O \cdot x(SiO_2)$
Si - FROM $Na_2O \cdot x(SiO_2)$
$SO_4^=$ - FROM Na_2SO_4

Si - FROM SiO_2
Na - IN SiO_2
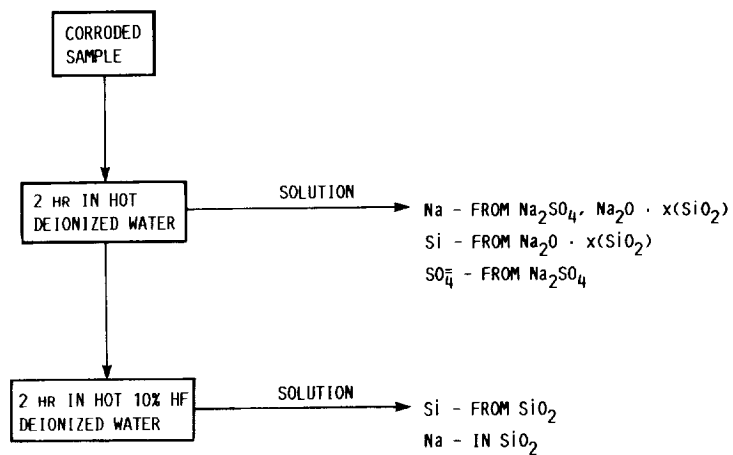
FIGURE 7. - CHEMICAL ANALYSIS SCHEME FOR DETERMINING COMPOSITION OF
CORROSION PRODUCTS ON SiC.
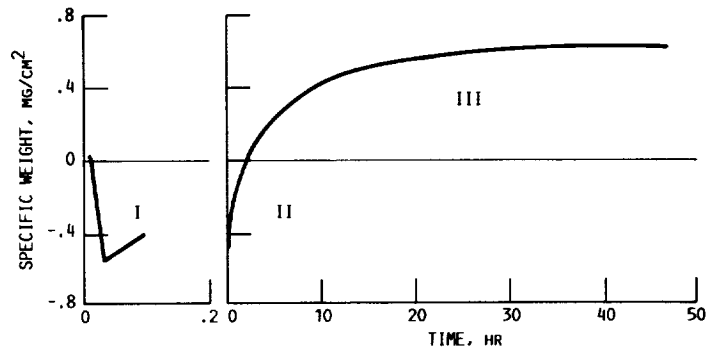
(a) THERMOGRAVIMETRIC ANALYSIS.
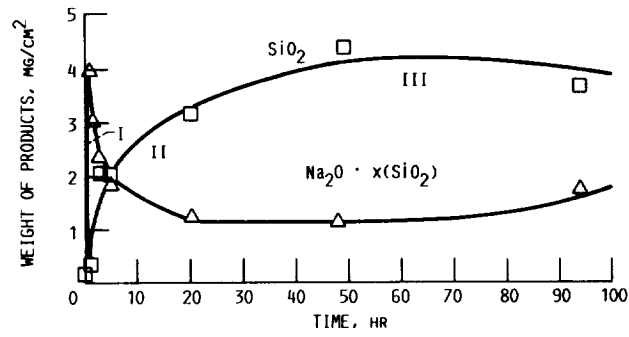
(b) CHEMICAL ANALYSIS.

FIGURE 8. - KINETIC CURVES FOR THE REACTION OF SASC (B,C) + Na_2CO_3/O_2 AT 1000 $^{\circ}C$.
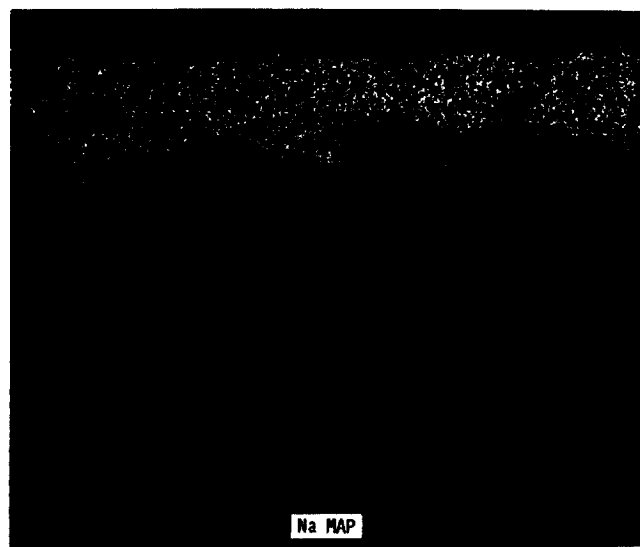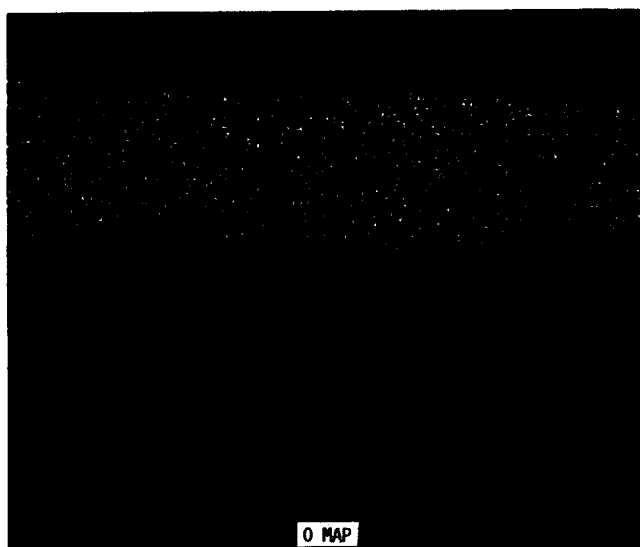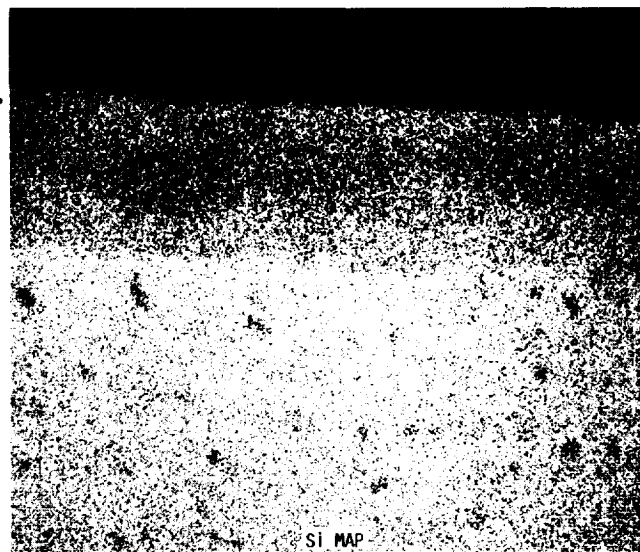
FIGURE 9. - ELECTRON MICROPROBE ANALYSIS OF A POLISHED CROSS SECTION OF CORROSION PRODUCTS FORMED FROM THE REACTION OF SASC (B,C) + Na_2CO_3/O_2 AT 1000 $^\circ$C FOR 48 HR.
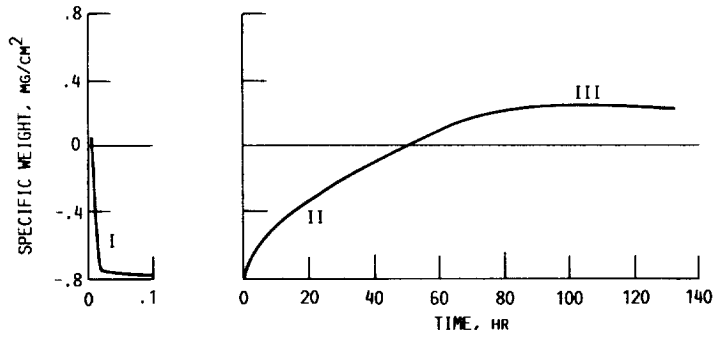
FIGURE 10. - TGA CURVE FOR SSN (Y_2O_3) + Na_2CO_3/O_2 AT 1000 ^oC.
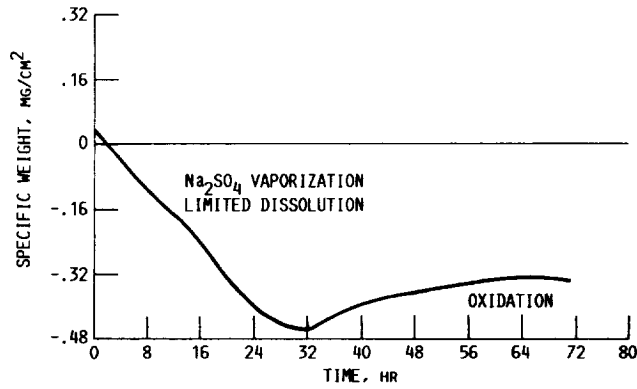
FIGURE 11. - TGA CURVE FOR HIP RBSN + Na_2SO_4/O_2 AT 1000 ^oC.
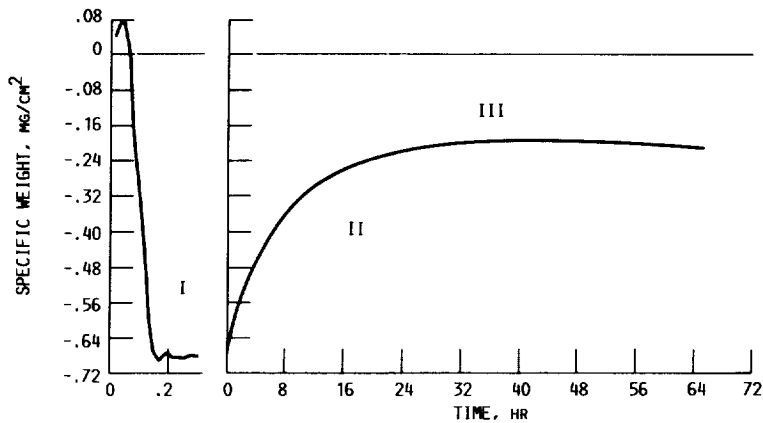
FIGURE 12. - TGA CURVE FOR SASC (B.C) + Na_2SO_4/O_2 AT
1000 ^oC.

56
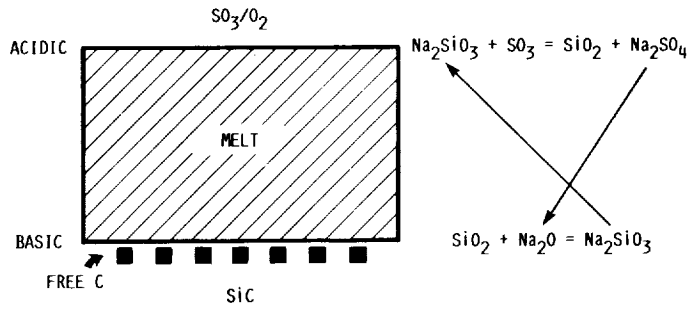
FIGURE 13. - SCHEMATIC OF FLUXING MECHANISM OPERATIVE IN SASC (B,C) + Na_2SO_4/SO_3.
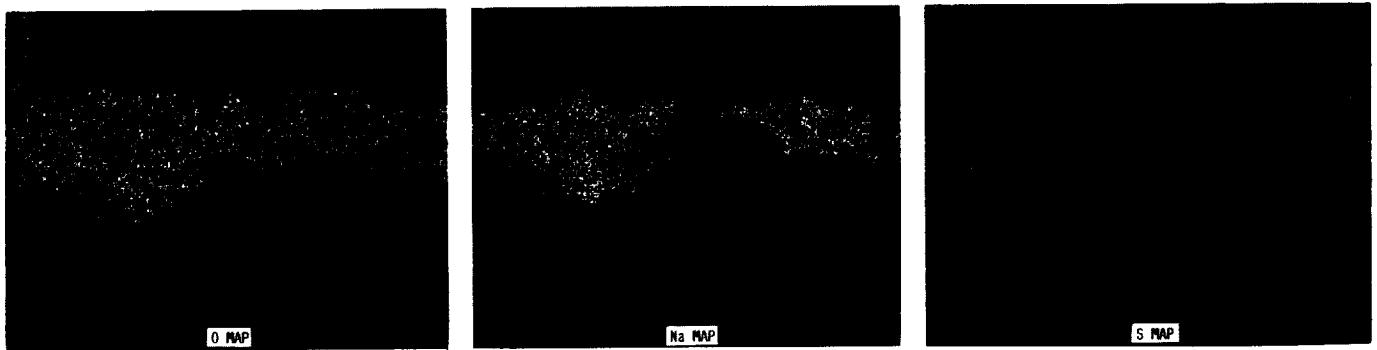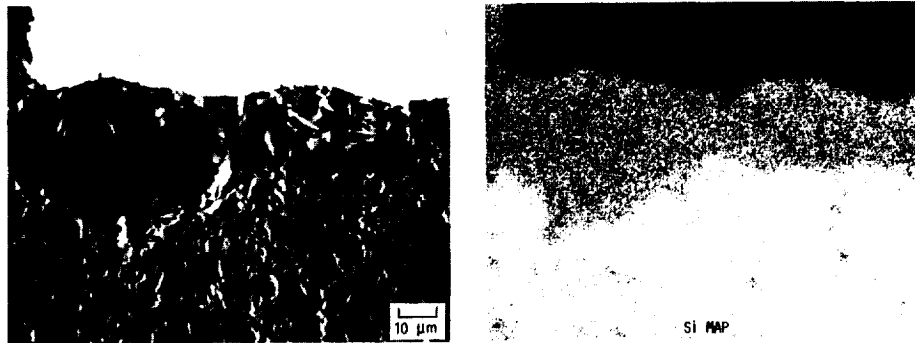
FIGURE 14. - ELECTRON MICROPROBE ANALYSIS OF A POLISHED CROSS SECTION OF CORROSION PRODUCTS FORMED FROM THE REACTION OF SASC (B,C) + Na_2SO_4/SO_3 AT 1000 °C FOR 20 HR.

BEFORE CORROSION

AFTER CORROSION

PRODUCTS REMOVED WITH HF
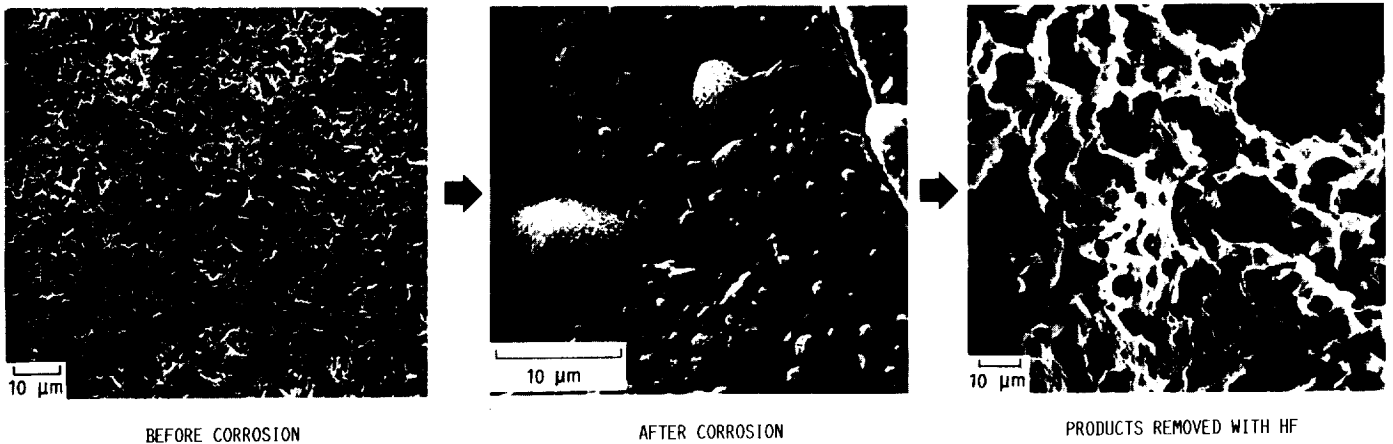
FIGURE 15. - SEQUENCE SHOWING SASC (B,C) BEFORE CORROSION, AFTER CORROSION WITH Na_2SO_4/SO_3 AT 1000 °C FOR 48 HR, AND WITH THE CORROSION PRODUCTS REMOVED WITH HF.

57

(a) AS-CORRODED SURFACE SHOWS BUBBLES AND PORES IN THE SILICATE LAYER.

(b) WATER LEACH REVEALS BUBBLES AND PORES IN THE SILICA LAYER.
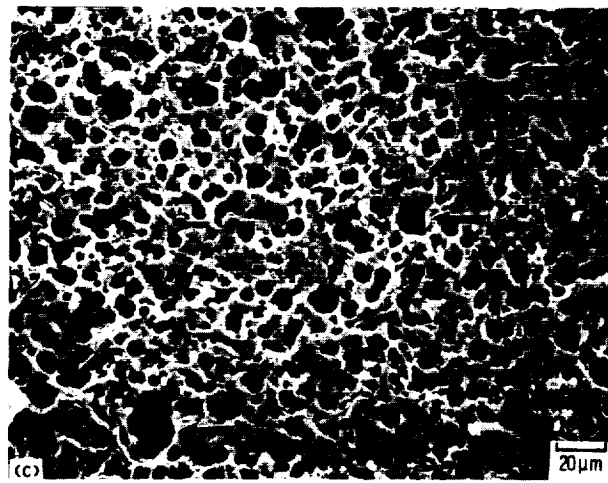
(c) HF LEACH SHOWS THE CORRELATION OF THESE BUBBLES AND PORES TO SOME OF THE PITS IN THE CERAMIC, AS SHOWN BY THE THREE ARROWS.

FIGURE 16. - SEM PHOTOS OF SASC (B,C) + 4.07 MG Na_2CO_3/cm^2 REACTED FOR 1 HR AT 1000 ^{o}C.
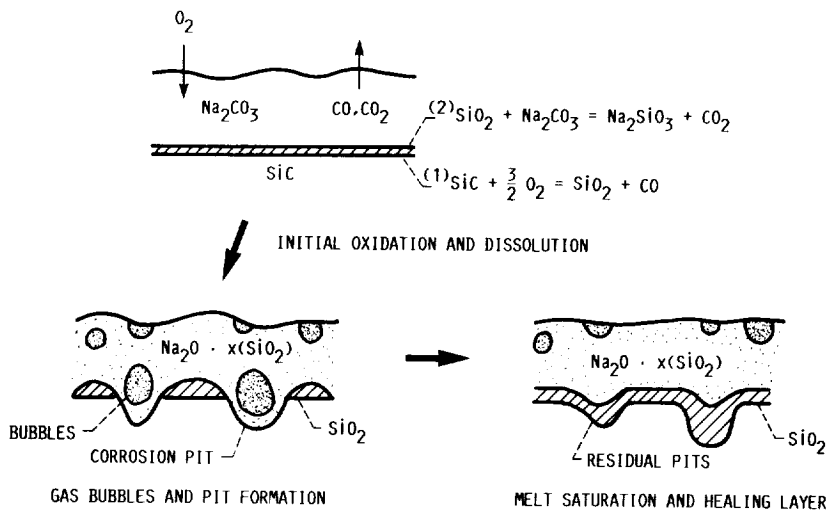
FIGURE 17. - SCHEMATIC OF PROPOSED PITTING MECHANISM IN SiC VIA BUBBLES.

BEFORE CORROSION   AFTER CORROSION   PRODUCTS REMOVED WITH HF
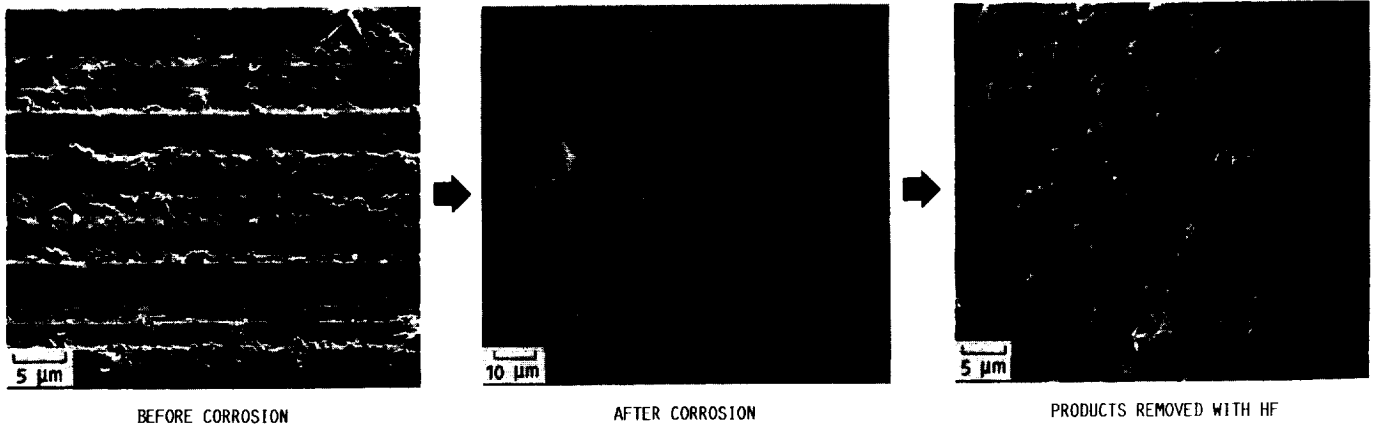
FIGURE 18. - SEQUENCE SHOWING SSN (Y_2O_3, Al_2O_3) BEFORE CORROSION, AFTER CORROSION WITH Na_2SO_4/O_2 AT 1000 ^oC FOR 48 HR, AND WITH THE CORROSION PRODUCTS REMOVED WITH A MILD HF TREATMENT.
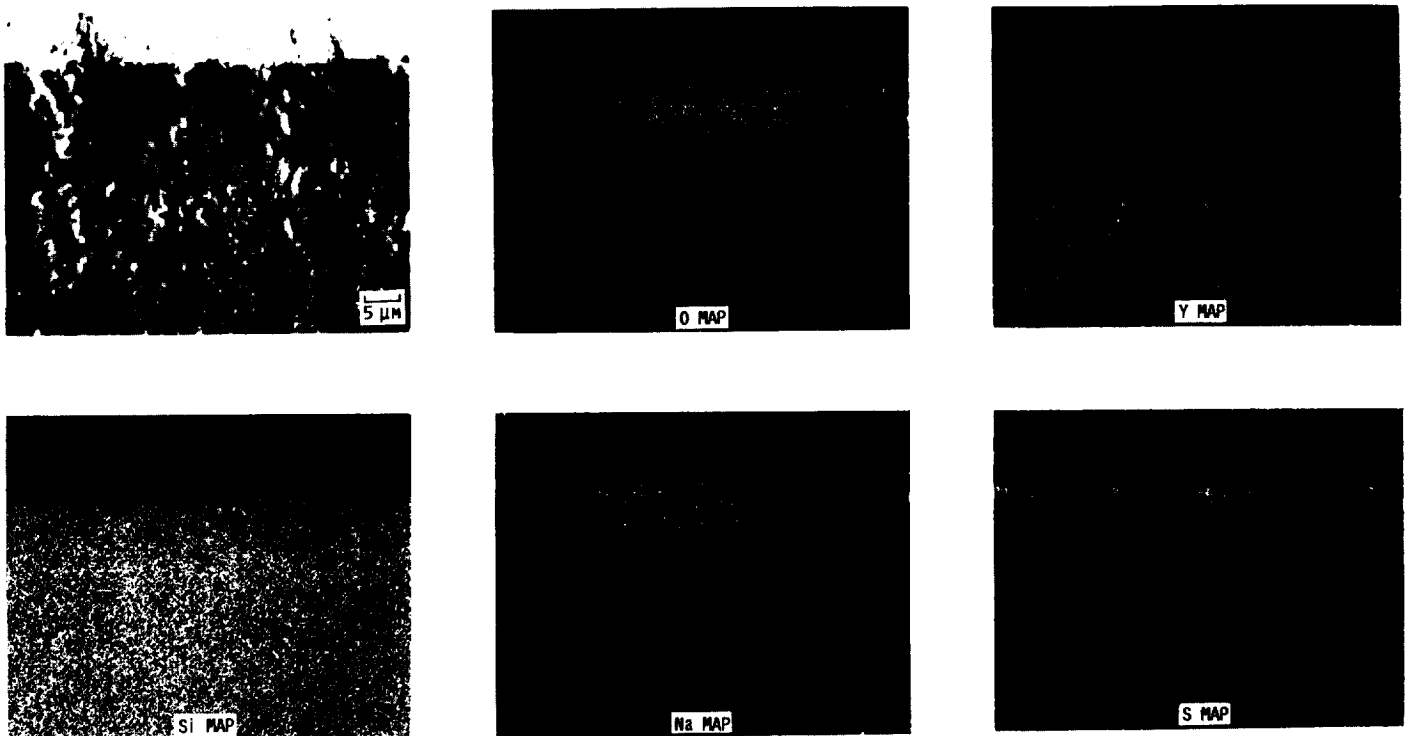
FIGURE 19. - ELECTRON MICROGRAPHS ANALYSIS SHOWING Y DEPLETION IN OUTER REGIONS OF SSN (Al_2O_3, Y_2O_3) WHEN REACTED WITH Na_2SO_4/O_2 FOR 48 HR AT 1000 ^oC.

59
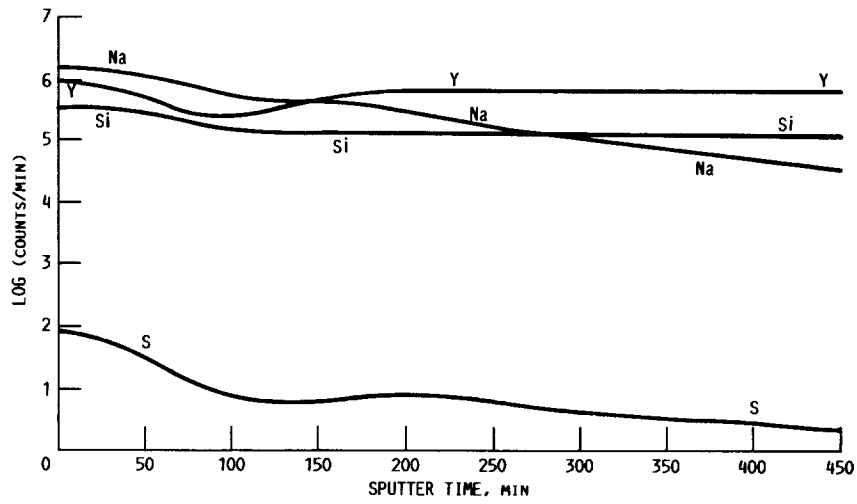
FIGURE 20. - SIMS PROFILE FOR SSN (Al_2O_3, Y_2O_3) + Na_2SO_4/O_2 REACTED AT 1000 °C FOR 48 HR. ANGLE LAPPED SPECIMEN, PROFILING STARTED AT SCALE/NITRIDE INTERFACE, FOR A TOTAL DEPTH OF 45 μM AFTER 450 MIN SPUTTER TIME.
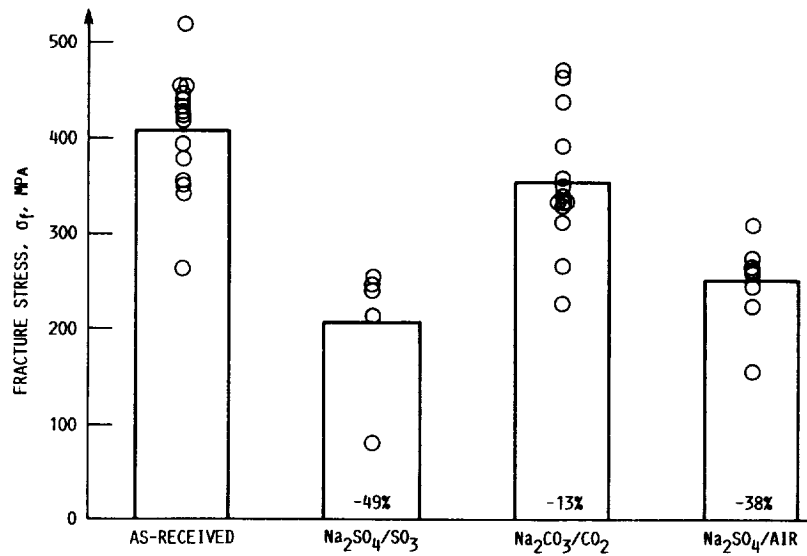
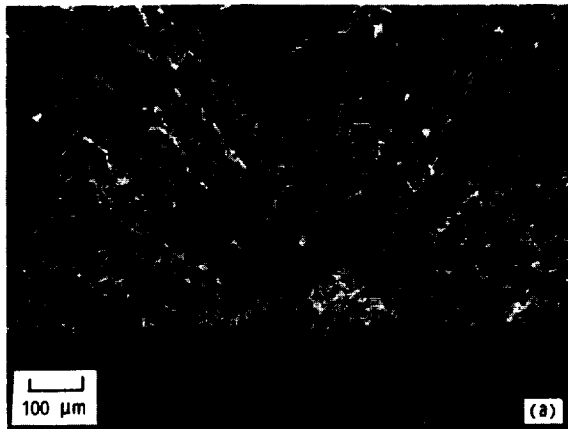FIGURE 21. - STRENGTH DEGRADATION OF SASC (B,C) AFTER FURNACE CORROSION TESTING FOR 48 HR AT 1000 °C.

60
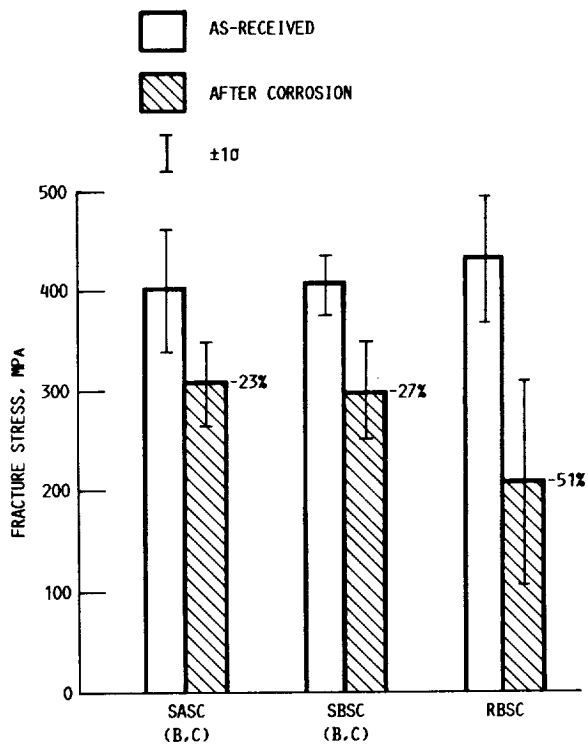
FIGURE 22. - STRENGTH DEGRADATION OF SiC AFTER BURNER RIG CORROSION AT 1000 °C (400 kPa, 2 ppm Na, JET A FUEL, 40 hr).

(a) RADIAL CRACK LINES EXTENDING TO THE ORIGIN.

(b) HONEYCOMB CORROSION PIT AT THE ORIGIN.

(c) PREFERENTIAL GRAIN BOUNDARY ATTACK AHEAD OF PIT IN (B).

FIGURE 23. - CORROSION PIT FRACTURE ORIGIN IN SASC (B,C) AFTER Na_2SO_4/SO_3 CORROSION AT 1000 ^{O}C FOR 48 HR.

62
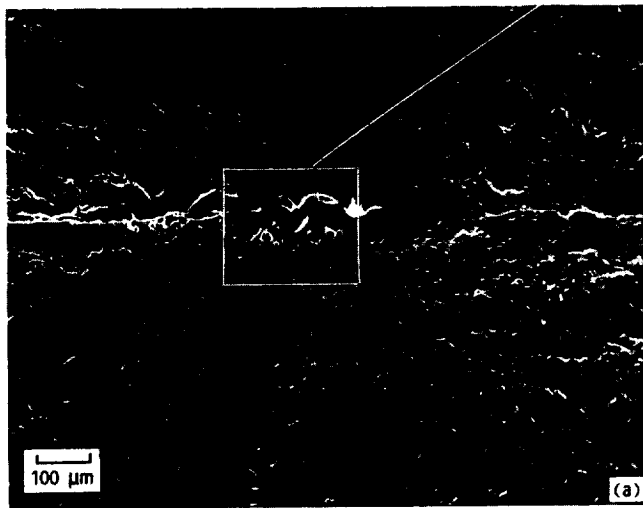
(a) MATTING HALVES OF FRACTURE ORIGIN.

(b) GLASSY PRODUCT AT ORIGIN.
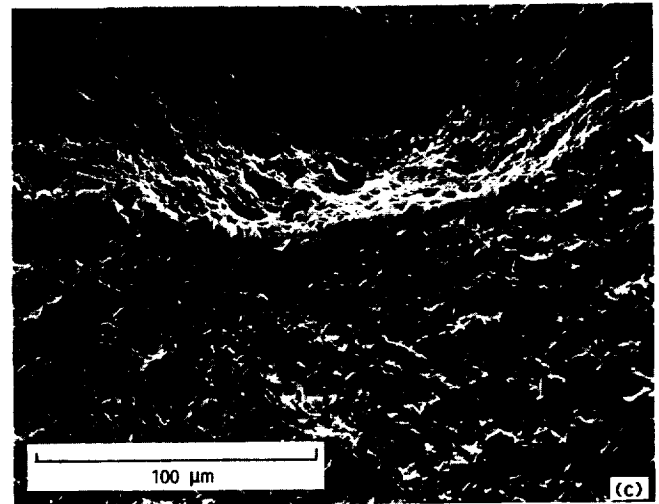
(c) PITTING AT ORIGIN REVEALED BY HF DISSOLUTION OF GLASSY PRODUCT.

FIGURE 24. – CORROSION PIT FRACTURE ORIGIN FOR A BURNER RIG CORRODED SASC (B,C) USING JET A FUEL, 4 PPM Na, 13.5 HR EXPOSURE AT 1000 °C.
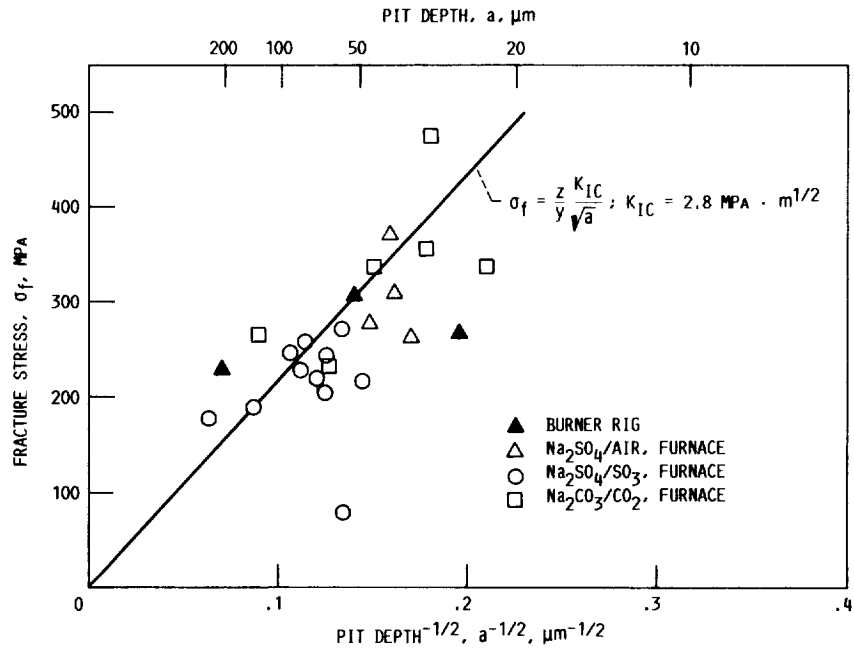
FIGURE 25. - CORRELATION OF FRACTURE STRENGTH WITH CORROSION PIT DEPTH, SASC (B,C) CORRODED IN BOTH THE FURNACE AND BURNER RIG.

The plot shows PIT DEPTH, a, μm on the top axis and FRACTURE STRESS, σ_f, MPa on the vertical axis. The relation shown is:

$$\sigma_f = \frac{z}{y}\frac{K_{IC}}{\sqrt{a}} \; ; \; K_{IC} = 2.8 \text{ MPa} \cdot \text{m}^{1/2}$$

Legend:
▲ BURNER RIG
△ Na_2SO_4/AIR, FURNACE
○ Na_2SO_4/SO_3, FURNACE
□ Na_2CO_3/CO_2, FURNACE

Bottom axis: PIT DEPTH$^{-1/2}$, $a^{-1/2}$, μm$^{-1/2}$

(a) SSN (Al_2O_3, Y_2O_2).
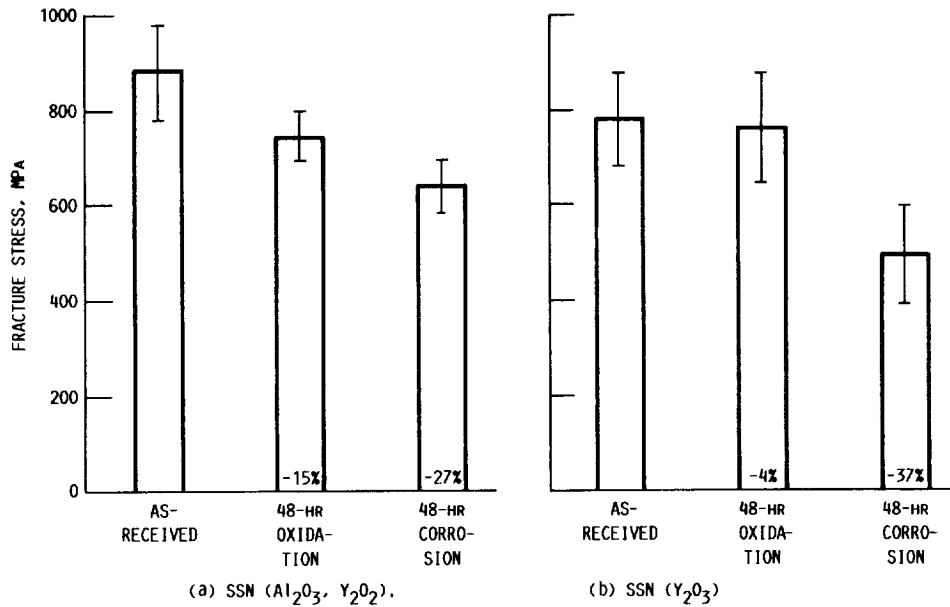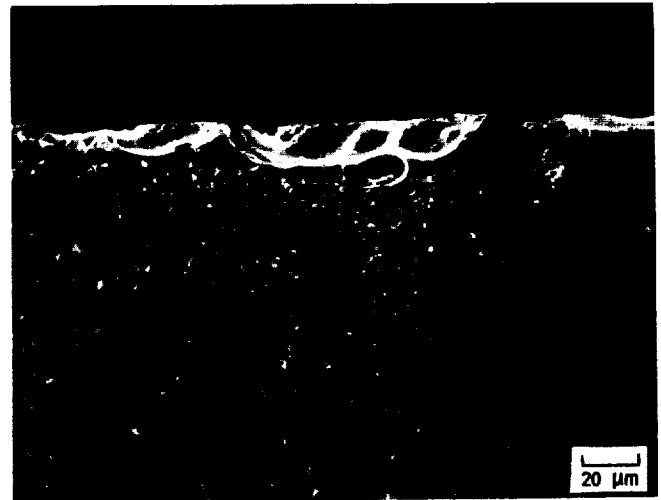
(b) SSN (Y_2O_3)

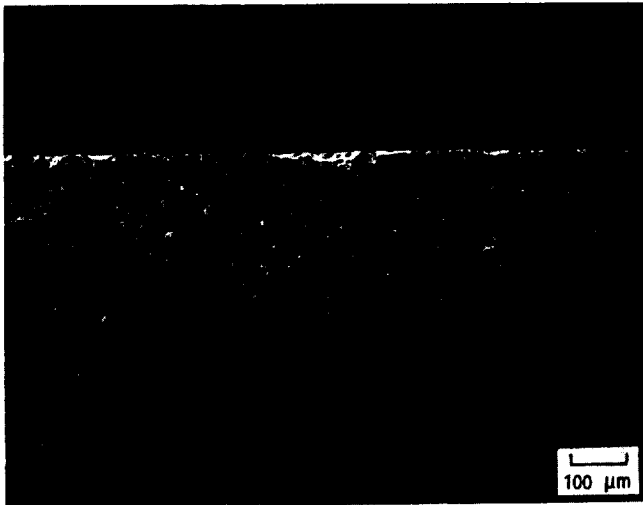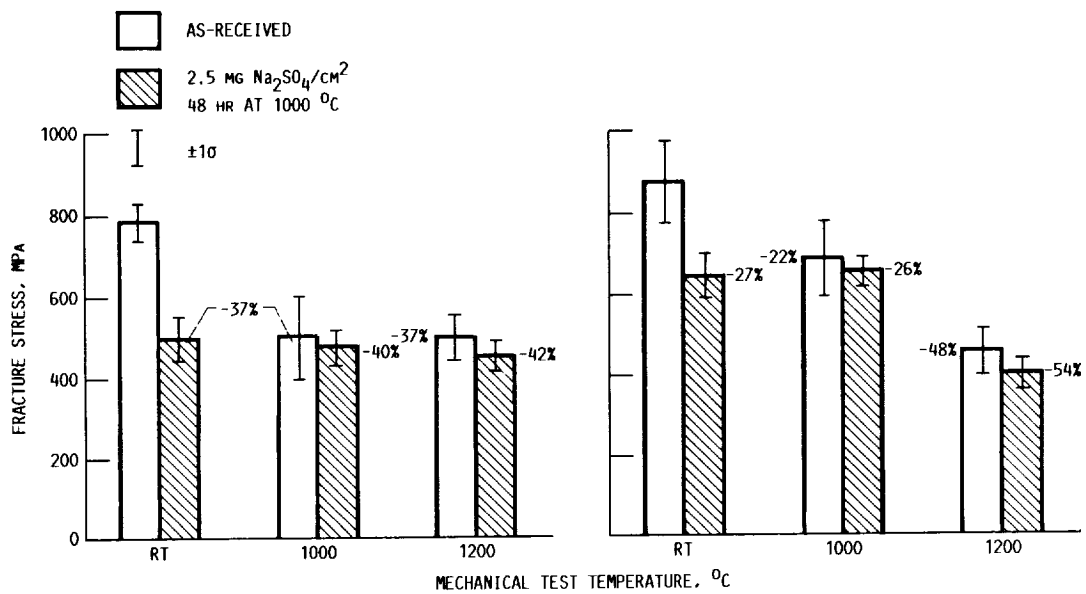FIGURE 26. - ROOM TEMPERATURE STRENGTHS. EACH MATERIAL AFTER 48 HR OF OXIDATION AT 1000 °C, AND EACH MATERIAL AFTER 48 HR OF CORROSION WITH Na_2SO_4/O_2 AT 1000 °C.
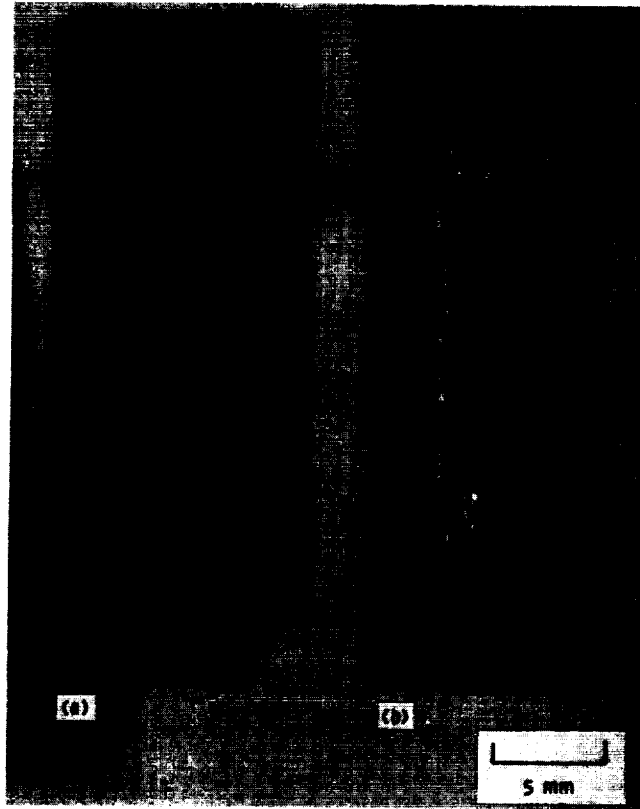
(a) OVERALL VIEW.

(b) ENLARGEMENT OF CORROSION SCALE AND BUBBLES AT ORIGIN.

FIGURE 27. - FRACTURE ORIGIN FOR SSN (Al_2O_3, Y_2O_3) + Na_2SO_4/O_2 CORRODED AT 1000 °C FOR 48 HR.

(a) SSN (A $_2O_3$, Y_2O_3).

(b) SSN (Y_2O_3).

FIGURE 28. - STRENGTH AND AS-RECEIVED AND CORRODED SSN MATERIALS AT ROOM TEMPERATURE, 1000 AND 1200 °C.

65

(a) WITH A DENSE MULLITE   (b) UNCOATED.
    PLASMA SPRAYED COATING.

FIGURE 29. - VIEWS OF SASC (B,C) TESTED IN THE BURNER RIG WITH JET A
    FUEL, 2 PPM Na, AT 1000 °C FOR 20 HR.

Report Documentation Page

1. Report No. NASA TM-101346	2. Government Accession No.	3. Recipient's Catalog No.
4. Title and Subtitle Molten Salt Corrosion of SiC and Si$_3$N$_4$		5. Report Date November 1988
		6. Performing Organization Code
7. Author(s) Nathan S. Jacobson, James L. Smialek, and Dennis S. Fox		8. Performing Organization Report No. E-4370
		10. Work Unit No. 505-63-1A
9. Performing Organization Name and Address National Aeronautics and Space Administration Lewis Research Center Cleveland, Ohio 44135-3191		11. Contract or Grant No.
		13. Type of Report and Period Covered Technical Memorandum
12. Sponsoring Agency Name and Address National Aeronautics and Space Administration Washington, D.C. 20546-0001		14. Sponsoring Agency Code

15. Supplementary Notes

This material in this report also appears in a chapter in the Encyclopedia of Engineering Materials.

16. Abstract

Industrial systems such as heat engines and heat exchangers involve harsh environments. The structural materials are subjected to high temperatures as well as corrosive gases and condensed phases. Past experience with metal alloys has shown that these condensed phases can be particularly corrosive and are often the limiting factor in the operation of these systems. In a heat engine the most common condensed corrodent is Na$_2$SO$_4$ whereas in a heat exchanger an oxide slag may be present. The primary emphasis of this chapter is on Na$_2$SO$_4$ induced corrosion, however similarities and differences to oxide slag corrosion are also discussed. The extensive research on corrosion of metal alloys has led to understanding and controlling corrosion for these materials. Currently silicon based ceramics are prime candidates for the applications discussed above. Therefore it is important to understand the effects of condensed phase deposits on this emerging class of high temperature materials. Both the thermodynamic and kinetics of the corrosion reactions are discussed. The effect of these corrosion reactions on the microstructure and strength of the ceramic is also examined. Finally some control strategies for corrosion of silicon based ceramics are explored.

17. Key Words (Suggested by Author(s)) Molten salt Corrosion Ceramics	18. Distribution Statement Unclassified – Unlimited Subject Category 27

19. Security Classif. (of this report) Unclassified	20. Security Classif. (of this page) Unclassified	21. No of pages 68	22. Price* A04